



Contents lists available at ScienceDirect



Tectonophysics

journal homepage: www.elsevier.com/locate/tecto

Eocene Neotethyan slab breakoff in southern Tibet inferred from the Linzizong volcanic record

Hao-Yang Lee ^{a,*}, Sun-Lin Chung ^a, Ching-Hua Lo ^a, Jianqing Ji ^b, Tung-Yi Lee ^c, Qing Qian ^d, Qi Zhang ^d^a Department of Geosciences, National Taiwan University, P. O. Box 13-318, Taipei 10617, Taiwan^b School of Earth and Space Sciences, Peking University, Beijing, China^c Department of Earth Sciences, National Taiwan Normal University, Taipei, Taiwan^d Institute of Geology and Geophysics, Chinese Academy of Sciences, Beijing, China

ARTICLE INFO

Article history:

Received 9 May 2008

Received in revised form 17 January 2009

Accepted 24 February 2009

Available online xxxx

Keywords:

Linzizong volcanism

Tibet

Neotethyan subduction

Slab breakoff

India–Asia collision

ABSTRACT

Formation of the Linzizong volcanic successions in the Lhasa terrane, southern Tibet has long been related to northward subduction of the Neotethyan oceanic slab under Asia. Here we report new $^{40}\text{Ar}/^{39}\text{Ar}$ age results for the volcanic rocks recovered from a large area (29°N to 32°N and 85°E to 93°E) that, together with literature data, delineate two discrete stages of volcanism. These are a widespread Cretaceous stage and an intense, but spatially confined, Paleogene stage. The latter, occurring only in the southern part of the Lhasa terrane, resulted in the Linzizong volcanic successions. Our data, furthermore, suggest southward migration and intensification of the volcanism in the Lhasa terrane with magmatic “flare-ups” at ca. 50 Ma. While the volcanic successions consist dominantly of calc-alkaline rocks typical of arc lava geochemistry, those formed during the flare-up period show significant compositional variations from low-K tholeiitic through calc-alkaline to shoshonitic magma suites. These observations enable us to interpret the volcanic southward migration and following flare-ups as the consequences of rollback and breakoff of the subducted Neotethyan slab that occurred ahead and in the early stage, respectively, of the India–Asia collision. Our interpretation that involves a major Eocene tectonomagmatic activity, and concomitant topographic uplift, in southern Tibet is consistent with Himalayan metamorphic constraints, regional sedimentary records and seismic tomography.

Crown Copyright © 2009 Published by Elsevier B.V. All rights reserved.

1. Introduction

The Himalayan–Tibetan orogen, formed by the collision of India with Asia, is the most outstanding natural laboratory for studying the complex geologic processes through which collisional orogenesis evolves (cf. Yin and Harrison, 2000). Before the collision, northward subduction of the Neotethyan oceanic lithosphere under South Asia gave rise to an Chilean/Andean type convergent margin (Coulon et al., 1986). Extensive igneous rocks thus produced in southern Tibet are now exposed as the Linzizong volcanic successions and Gangdese batholith in the Lhasa terrane, north of the Yarlu Tsangpo suture zone (Fig. 1). In the terminal stage of this subduction, or its transition to the India–Asia collision, which may have involved attempted continental subduction (Chemenda et al., 2000), breakoff of the subducted Neotethyan oceanic slab from the adherent, more buoyant Indian continental lithosphere would have taken place as a result of gravitational resetting and strain localization (cf. Davies and von Blanckenburg, 1995). The timing and consequence of the slab breakoff in the Himalayan–Tibetan evolution have therefore attracted attention,

such that it has been proposed as occurring in either the Eocene (e.g., DeCelles et al., 2002; Kohn and Parkinson, 2002; Guillot et al., 2003; Chung et al., 2005) or the Oligocene–Miocene (e.g., Miller et al., 1999; Mahéo et al., 2002; Aitchison et al., 2007), corresponding specifically to the Eohimalayan metamorphism and the potassic magmatism in southern Tibet, respectively. By conducting a detailed geochronological study combined with petrochemical analyses, we report here for the first time the temporal–spatial and geochemical systematics of the Linzizong volcanism. The new data identify a significant igneous “flare-up” record in southern Tibet for constraining not only the Neotethyan subduction but also the geodynamic evolution in the region.

2. Geologic background and samples

The Linzizong volcanic successions represent one of the most striking features in southern Tibet. The successions occur largely as pyroclastics, lava flows and ignimbrites in an elongated area of $\sim 1000 \times 200$ km, with thickness varying from >2500 to several hundred meters (Coulon et al., 1986; Pan et al., 2004), and are particularly well exposed in the central part of the southern Lhasa terrane (Fig. 1). In addition, they are essentially flat-lying or only

* Corresponding author. Tel.: +886 2 3366 2933; fax: +886 2 2363 6095.

E-mail address: haoyanglee@ntu.edu.tw (H.-Y. Lee).

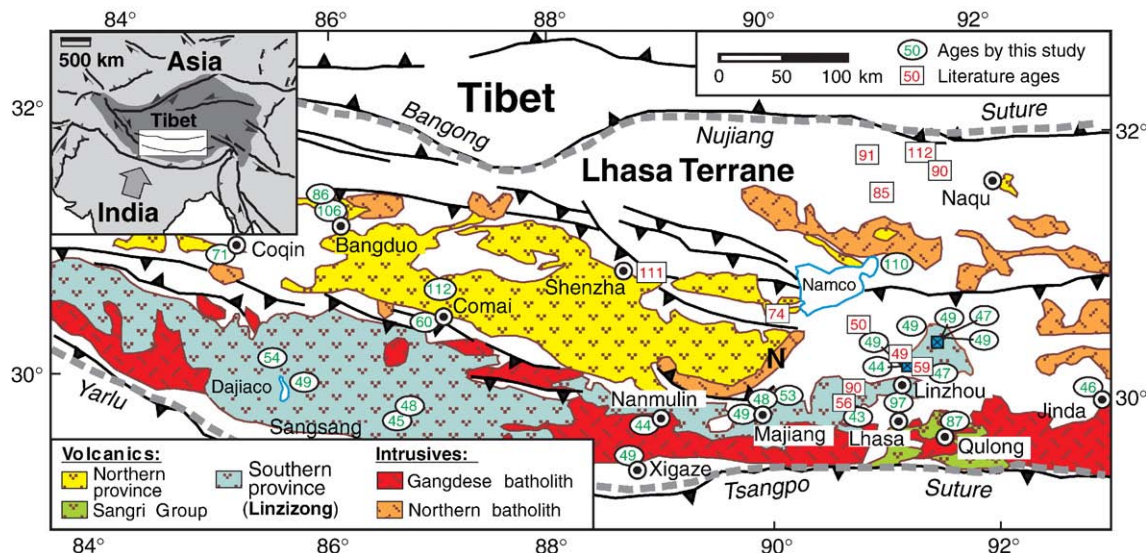


Fig. 1. Geologic map (after Yin and Harrison, 2000; Pan et al., 2004) showing distribution and eruption ages of major igneous rocks in the Lhasa terrane, southern Tibet. Literature age data are from Coulon et al. (1986).

slightly tilted on more strongly deformed Mid-Cretaceous or older strata. This led some workers (e.g., Yin and Harrison, 2000) to argue that the Lhasa terrane had not experienced significant north–south shortening in the upper crust since the early Cenozoic. Limited amounts of age data reported by the Sino-French pioneer work (Maluski et al., 1982; Coulon et al., 1986) and studies afterwards (e.g., Murphy et al., 1997; Mo et al., 2003; Lee et al., 2007; He et al., 2007) from restricted areas indicate that the eruptions took place during Early Paleogene time although stratigraphic constraints show some minor eruptions in the Late Cretaceous (Pan et al., 2004). Despite lacking detailed petrochemical investigations, the Linzizong volcanism has long been genetically linked with the temporal–spatially associated Gangdese plutonism and hence attributed to the Neotethyan subduction.

In our study, various types of volcanic samples were collected via five N–S transects in a rectangular area from 29°N to 32°N and 85°E to 93°E in the Lhasa terrane (Fig. 1). Among a total of 90+ samples subjected to detailed geochemical analyses involving whole-rock major and trace element and Sr–Nd isotope measurements (Lee, 2007), 26 whole-rock samples ranging from basalt to rhyolite were selected for $^{40}\text{Ar}/^{39}\text{Ar}$ age dating. These include samples from (1) the northern part of the Linzizong volcanic successions, following Yin and Harrison (2000) for the areal distribution, hereafter coined as “the northern province”, (2) the southern part of the Linzizong successions, hereafter referred as “the southern province”, and (3) the Sangri Group that crops out in the southeast of Lhasa city in the southern province (Fig. 1). This paper explores the temporal–spatial distribution of the volcanic rocks and its geodynamic implications, based largely upon our new $^{40}\text{Ar}/^{39}\text{Ar}$ age results and geochemical constraints. Detailed discussion on the full set of geochemical and isotopic data that is beyond the scope of this paper will be given in a separate article.

3. $^{40}\text{Ar}/^{39}\text{Ar}$ geochronology

3.1. Methodology

Whole-rock chips were crushed and sieved to size of 20–40 mesh (850–425 μm), ultrasonically cleaned in distilled water and dried, and handpicked under a stereoscope to remove visible impurities. Aliquots of about 400 mg, together with a monitor standard, LP-6 Biotite (128.4 ± 0.2 Ma; Renne et al., 1998) of weighted 6–10 mg, were

irradiated using the Tsing-Hua Open Pool Reactor (THOR) in Taiwan (cf. Lo et al., 2002). After irradiation, the standard and samples were degassed using a double-vacuum resistance furnace in steps from 600 to 1600 °C with a 30-min heating schedule or using a defocused Nd-YAG laser system (US LASER) in steps by increasing energy. Furnace temperatures were calibrated to ± 2 °C. Argon isotopes were measured using Varian-MAT GD150 and VG3600 mass spectrometers at National Taiwan University. Isotopic results were corrected for mass discrimination, interfering nuclear reactions, procedural blanks and atmospheric argon contamination. Dates were obtained by using the following equations:

$$\text{Date} = \frac{1}{\lambda} \ln \left(1 + J \frac{^{40}\text{Ar}^*}{^{39}\text{Ar}_K} \right), \text{ and}$$

$$\frac{^{40}\text{Ar}^*}{^{39}\text{Ar}_K} = \frac{\left[^{40}\text{Ar} / ^{39}\text{Ar} \right]_m - 295.5 \left[^{36}\text{Ar} / ^{39}\text{Ar} \right]_m + 295.5 \left[^{36}\text{Ar} / ^{37}\text{Ar} \right]_{\text{Ca}} \left[^{37}\text{Ar} / ^{39}\text{Ar} \right]_m}{1 - \left[^{39}\text{Ar} / ^{37}\text{Ar} \right]_{\text{Ca}} \left[^{37}\text{Ar} / ^{39}\text{Ar} \right]_m} - \left[\frac{^{40}\text{Ar}}{^{39}\text{Ar}} \right]_K$$

where λ = decay constant from Steiger and Jäger (1977), J = neutron flux calculated using argon compositions of the LP-6 standard and calibrated by Fish Canyon sanidine (28.02 ± 0.28 Ma; Renne et al., 1998), $[]_{\text{Ca}}$ and $[]_K$ = isotope ratios of argon extracted from irradiated calcium and potassium salts, and $[]_m$ = isotope ratio of argon extracted from irradiated unknown. Plateau ages are defined for the dates and errors calculated from the sum total gas comprising three or more continuous heating steps and corresponding to at least 50% of the total ^{39}Ar released, and the individual fraction ages overlap at 2σ confidence level (Fleck et al., 1977). More detailed analytical conditions and procedures can be found in Lo et al. (2002) and Lee et al. (2003).

3.2. $^{40}\text{Ar}/^{39}\text{Ar}$ results

Our dating results are summarized in Table 1, with whole set of detailed data being listed in Table 2 and displayed using age spectra in Figs. 2 and 3. These results, indicated also in the geologic map (Fig. 1), were combined with published age data (Table 3) to construct the histograms of age distribution (Fig. 4).

Table 1Summary of whole-rock $^{40}\text{Ar}/^{39}\text{Ar}$ dating results.

Locality	Sample	Latitude, longitude ($^{\circ}\text{N}$, $^{\circ}\text{E}$)	Rock type (suite ^a)	N (steps)	^{39}Ar proportion (%)	Plateau age (Myr $\pm 2\sigma$)
<i>Southern province (Linzizong)</i>						
Linzhou	ST053	30.11, 91.28	Dacite (Sh)	14	100	47.1 \pm 0.6
Linzhou	ST055A	30.16, 91.25	Rhyolite (Sh)	10	75.6	49.3 \pm 0.6
Linzhou	ST055C	30.16, 91.25	Basaltic andesite (Sh)	9	85.5	43.8 \pm 0.6
Linzhou	ST057A	30.29, 91.41	Andesite (Sh)	12	95.9	46.5 \pm 0.6
Linzhou	ST059A	30.23, 91.36	Dacite (Sh)	5	58.1	48.8 \pm 0.6
Linzhou	ST060C	30.20, 91.34	Dacite (Sh)	6	71.2	48.7 \pm 1.0
Linzhou	ST062	30.27, 91.24	Dacite (Sh)	10	88.7	48.5 \pm 0.8
Xigaze	T041F	29.36, 88.81	Basaltic andesite (low-K)	6	63.3	49.3 \pm 1.2
Nanmulin	T047	29.67, 89.08	Basalt (C-A)	11	85.1	44.0 \pm 0.8
Maijiang	T065A	29.74, 89.88	Rhyolite (C-A)	8	63.1	48.6 \pm 2.2
Maijiang	T068	29.73, 89.98	Rhyolite (C-A)	9	92.8	47.8 \pm 1.8
W Lhasa	T083C	29.77, 90.78	Basalt (C-A)	6	66.3	43.2 \pm 1.6
NE Maijiang	T105A	29.90, 90.13	Andesite (C-A)	4	72.4	53.0 \pm 0.8
Jinda	T006B1	29.99, 93.04	Basaltic andesite (C-A)	8	52.4	45.7 \pm 1.8
N Sangsang	T038F	29.65, 86.70	Dacite (C-A)	10	98.6	47.7 \pm 2.2
N Sangsang	T038G	29.65, 86.70	Dacite (C-A)	11	95.8	45.1 \pm 1.6
Dajiaco	T155	29.90, 85.74	Dacite (C-A)	7	50.1	48.9 \pm 0.8
NW Dajiaco	T151	30.23, 85.32	Basalt (C-A)	9	80.9	53.9 \pm 1.0
Comai	T136A	30.51, 87.06	Rhyolite (C-A)	14	97.6	59.9 \pm 0.8
<i>Northern province</i>						
N Comai	T131A	30.65, 87.06	Rhyolite	4	67.2	112 \pm 3
Bangduo	T139	31.35, 85.90	Rhyolite	4	65.5	85.8 \pm 1.0
Bangduo	T140B	31.34, 85.88	Andesite	7	61.3	106 \pm 2
Coqin	T142	30.98, 85.13	Dacite	8	68.1	71.1 \pm 0.8
Namuco	T169A	30.85, 91.14	Rhyolite	12	89.4	110 \pm 1
<i>Sangri Group</i>						
Lhasa-NE	T078B	29.91, 91.23	Dacite	6	69.2	97.3 \pm 2.0
Qulong	ET022A	29.52, 91.51	Rhyolite	5	55.9	87.2 \pm 1.4

Analytical details are given in Table 2.

^a Sh: shoshonitic; C-A: median- to high-K calc-alkaline; low-K: low-K tholeiitic.

The spectra of all 26 dated samples yielded “plateau ages” following the above-stated definitions (Table 1 and Figs. 2 and 3), and these plateau ages are adopted to represent the individual eruption ages. However, there are several samples that show complicated spectra, as detailed below, we tend to be more conservative in their age interpretations. Among all of these, 19 samples (basalt to rhyolite) from the southern province yielded a range of plateau dates between ca. 60 and 43 Ma, with 2σ errors of each sample being 0.6–2.2 Ma (Table 1 and Fig. 2). The first group of seven samples were collected from the Linzhou area (Fig. 2; a–g), the “type locality” of the Linzizong volcanic successions (cf. Pan et al., 2004). Notably, four of the seven samples (Fig. 2; a–d) yielded “reasonable” plateau ages (i.e., with age fractions overlapping at 2σ analytical errors) in a narrow span from ca. 49 to 44 Ma but display monotonically increasing age spectra. In contrast to the other three (Fig. 2; e–g) that show “truly” flat spectra yielding coeval plateau ages of ca. 49 Ma suggestive of eruption ages, the monotonically increasing age spectra may be ascribed to argon loss, as argued by He et al. (2007) that reported thermochronologic evidence indicating that these rocks were substantially buried during the Paleogene and thus could have undergone argon loss. If so, a significantly larger range of possible ages or age uncertainties should be considered for the complicated samples. For example, the eruption age of sample ST055C (Fig. 2c) that has an increasing age spectrum from ca. 40 to 46 Ma may be better regarded as 43 ± 3 Ma, with a greater corresponding uncertainty.

Similar ages (ca. 49–43 Ma) were obtained for a group of five samples from nearby areas around Xigaze, Nanmulin, Maijiang and Lhasa, respectively (Fig. 2; h–l). Two of them (Fig. 2; h and j), however, show concave-shaped age spectra with abnormally older ages at low- and high-temperature steps that we attribute to outgassing of excess argon and/or impurities. One basaltic lava has abnormally young dates in the first several percent of gas released (Fig. 2l), reflecting either the presence of impurities or argon loss. In addition, a slightly older but well-defined plateau date of ca. 53 Ma was obtained for an

andesitic lava flow from Maijiang (Fig. 2m). An andesitic dike recovered from Jinda in the easternmost part of this province (Fig. 2n) gave a U-shaped spectrum yielding a plateau age of ca. 46 Ma. In the west, 4 samples from Sangsang and Dajiaco areas (Fig. 2; o–r) yielded plateau ages between ca. 45 and 54 Ma. The latter two show a drastic drop of ages at low temperature steps, which may have resulted from argon loss. A basaltic lava from Comai in the northern part of the province (Fig. 2s) yielded an apparently older age of ca. 60 Ma.

By contrast, seven andesitic to rhyolitic rocks collected from the “northern province” and the Sangri Group show Cretaceous ages (Table 1 and Fig. 3). The former include five samples from areas around Comai, Bangduo, Coqin and Namuco (Fig. 3; a–e), which yielded well-defined plateau ages between ca. 71 and 112 Ma. Two others are from areas near Qulong and Lhasa (Fig. 3; f and g), both mapped as the Sangri Group of Late Jurassic to Early Cretaceous ages (cf. Pan et al., 2004) but yielding Late Cretaceous plateau ages of ca. 97 and 87 Ma. This indicates that the volcanic divisions in the areas need re-evaluation with more detailed investigations, because part of the rocks are actually of Late Cretaceous ages and thus erupted coevally with deposition of the Takena Formation (Leier et al., 2007). Alternatively, the ages could probably be cooling ages rather than crystallization ages, related to the movement of the Gangdese retroarc thrust belt (cf. Kapp et al., 2007a).

4. Whole-rock geochemistry

In addition to all 90+ volcanic samples plotted in Fig. 5 (data from Lee, 2007), major and trace element and Nd isotope data of representative volcanic samples are given in Table 4.

Major and trace element data indicate, as delineated in the K_2O vs. SiO_2 plots (Fig. 5a), that the entire volcanic successions are overwhelmed with median- to high-K calc-alkaline compositions. They all exhibit significant enrichments in the large ion lithophile elements (LILE; e.g., Rb and Ba), light rare earth elements (LREE) and lead,

Table 2Detailed $^{40}\text{Ar}/^{39}\text{Ar}$ dating results of the Linzizong and related volcanic rocks.

T(°C)	Cum. $^{39}\text{Ar}_K$ (%)	Atmos.	$^{36}\text{Ar}/^{39}\text{Ar}$	$^{37}\text{Ar}/^{39}\text{Ar}$	$^{38}\text{Ar}/^{39}\text{Ar}$	$^{40}\text{Ar}/^{39}\text{Ar}$	$^{40}\text{Ar}/^{36}\text{Ar}$	Date (Ma) $\pm 1\sigma$
<i>Southern province (Linzizong)</i>								
600	0.023	46.915	2.20E–02	2.62E+00	8.78E–02	1.35E+01	6.12E+02	43.5 \pm 3.3
650	0.045	9.156	2.50E–03	2.59E–01	2.07E–02	7.88E+00	3.15E+03	43.4 \pm 0.5
700	0.119	6.516	1.68E–03	2.49E–01	1.91E–02	7.38E+00	4.38E+03	41.9 \pm 0.6
750	0.187	4.788	1.25E–03	8.49E–02	1.42E–02	7.60E+00	6.09E+03	43.8 \pm 0.3
800	0.321	8.020	2.21E–03	2.12E–01	1.79E–02	7.96E+00	3.61E+03	44.4 \pm 0.3
850	0.377	2.876	7.75E–04	1.30E–01	1.43E–02	7.65E+00	9.87E+03	45.1 \pm 0.4
900	0.440	2.571	7.08E–04	1.60E–01	1.39E–02	7.69E+00	1.09E+04	45.4 \pm 0.3
960	0.503	1.896	5.44E–04	1.80E–01	1.43E–02	7.79E+00	1.43E+04	46.3 \pm 0.3
1020	0.577	3.269	9.36E–04	1.71E–01	1.52E–02	8.10E+00	8.65E+03	47.5 \pm 0.3
1100	0.661	5.146	1.52E–03	1.65E–01	1.65E–02	8.51E+00	5.60E+03	48.9 \pm 0.4
1200	0.869	9.691	3.03E–03	1.66E–01	1.82E–02	9.13E+00	3.02E+03	50.0 \pm 0.3
1300	0.930	10.892	3.56E–03	1.43E–01	1.93E–02	9.58E+00	2.69E+03	51.7 \pm 0.3
1400	0.968	10.553	3.54E–03	2.22E–01	1.98E–02	9.78E+00	2.76E+03	53.0 \pm 0.5
1500	1.000	16.161	5.59E–03	3.06E–01	2.03E–02	1.01E+01	1.81E+03	51.3 \pm 0.5
Integrated date = 47.1 \pm 0.3 Ma								
Plateau date = 47.1 \pm 0.3 Ma (600–1500 °C)								
J-value = 0.003415284 \pm 0.000018960								
<i>ST055A</i>								
600	0.005	89.786	1.05E–01	6.57E–06	5.87E–02	3.46E+01	3.29E+02	21.6 \pm 2.3
650	0.054	53.929	2.10E–02	1.97E–01	2.89E–02	1.15E+01	5.48E+02	32.4 \pm 0.8
700	0.072	11.974	2.79E–03	1.51E–02	1.66E–02	6.90E+00	2.48E+03	36.9 \pm 0.9
750	0.099	9.579	2.38E–03	2.72E–02	1.72E–02	7.34E+00	3.09E+03	40.3 \pm 0.5
800	0.244	14.764	4.01E–03	8.11E–02	1.85E–02	8.01E+00	2.00E+03	41.4 \pm 0.3
850	0.269	5.912	1.64E–03	4.04E–03	1.74E–02	8.21E+00	5.01E+03	46.8 \pm 0.6
900	0.567	5.601	1.58E–03	6.08E–02	1.77E–02	8.25E+00	5.24E+03	47.2 \pm 0.5
960	0.608	7.735	2.26E–03	5.80E–02	1.87E–02	8.61E+00	3.81E+03	48.2 \pm 0.4
1020	0.645	10.427	3.16E–03	2.27E–02	2.11E–02	8.96E+00	2.84E+03	48.6 \pm 0.7
1100	0.710	15.391	4.98E–03	2.01E–02	2.33E–02	9.58E+00	1.92E+03	49.1 \pm 0.4
1200	0.823	27.438	1.07E–02	4.67E–02	2.94E–02	1.15E+01	1.08E+03	50.5 \pm 0.3
1300	0.846	44.358	2.33E–02	1.59E–06	3.33E–02	1.55E+01	6.67E+02	52.3 \pm 0.7
1400	0.874	40.214	1.98E–02	1.29E–06	3.11E–02	1.46E+01	7.36E+02	52.7 \pm 0.5
1500	0.972	39.338	1.94E–02	6.82E–02	3.14E–02	1.46E+01	7.52E+02	53.6 \pm 0.3
1600	1.000	43.197	2.19E–02	1.29E–06	3.11E–02	1.50E+01	6.85E+02	51.8 \pm 0.7
Integrated date = 46.8 \pm 0.3 Ma								
Plateau date = 49.3 \pm 0.3 Ma (850–1600 °C)								
J-value = 0.003415284 \pm 0.000018960								
<i>ST055C</i>								
600	0.007	65.436	4.38E–02	4.60E–01	3.43E–02	1.97E+01	4.51E+02	41.5 \pm 2.1
650	0.023	35.782	1.17E–02	5.37E–01	2.51E–02	9.58E+00	8.19E+02	37.4 \pm 1.2
700	0.082	6.259	1.90E–03	6.47E–01	2.82E–02	8.20E+00	4.33E+03	46.6 \pm 1.3
750	0.100	3.688	9.65E–04	3.74E–01	1.85E–02	6.99E+00	7.25E+03	40.9 \pm 1.0
800	0.141	4.123	1.09E–03	2.86E–01	1.59E–02	7.29E+00	6.71E+03	42.4 \pm 0.7
850	0.370	6.152	1.58E–03	2.39E–01	1.60E–02	7.33E+00	4.64E+03	41.7 \pm 0.6
900	0.398	3.932	1.04E–03	2.06E–01	1.51E–02	7.45E+00	7.16E+03	43.4 \pm 0.9
960	0.584	2.108	5.83E–04	1.97E–01	1.48E–02	7.50E+00	1.29E+04	44.5 \pm 0.4
1020	0.612	1.242	4.15E–04	4.14E–01	1.53E–02	7.40E+00	1.78E+04	44.3 \pm 0.4
1100	0.662	2.364	7.48E–04	6.04E–01	1.62E–02	7.45E+00	9.96E+03	44.1 \pm 0.4
1200	0.753	4.763	1.40E–03	5.55E–01	1.88E–02	7.86E+00	5.60E+03	45.4 \pm 0.4
1300	0.937	7.440	2.19E–03	6.20E–01	1.96E–02	8.11E+00	3.70E+03	45.5 \pm 0.3
1400	0.979	13.211	4.25E–03	8.27E–01	2.25E–02	9.07E+00	2.13E+03	47.7 \pm 0.5
1500	1.000	13.424	4.54E–03	8.44E–01	2.30E–02	9.54E+00	2.10E+03	50.1 \pm 0.7
Integrated date = 44.2 \pm 0.3 Ma								
Plateau date = 43.8 \pm 0.3 Ma (750–1300 °C)								
J-value = 0.003415284 \pm 0.000018960								
<i>ST057A</i>								
600	0.005	68.809	8.60E–02	4.36E–01	4.37E–01	3.69E+01	4.29E+02	69.6 \pm 4.7
650	0.041	41.232	2.15E–02	1.16E+00	1.97E–01	1.53E+01	7.08E+02	54.3 \pm 2.5
700	0.049	35.088	1.25E–02	7.67E–01	1.34E–01	1.04E+01	8.31E+02	41.1 \pm 2.7
750	0.066	31.538	1.11E–02	4.07E–01	1.20E–01	1.03E+01	9.31E+02	42.9 \pm 1.1
800	0.104	23.945	8.10E–03	2.66E–01	9.65E–02	9.95E+00	1.23E+03	45.9 \pm 0.4
850	0.254	18.657	5.79E–03	3.45E–01	7.70E–02	9.07E+00	1.57E+03	44.7 \pm 0.5
900	0.276	12.143	3.34E–03	4.36E–01	4.64E–02	7.89E+00	2.36E+03	42.1 \pm 1.1
960	0.315	7.660	2.08E–03	3.73E–01	3.78E–02	7.67E+00	3.70E+03	42.9 \pm 0.5
1020	0.377	3.745	1.04E–03	2.99E–01	3.90E–02	7.65E+00	7.34E+03	44.7 \pm 0.5
1100	0.487	6.039	1.72E–03	3.50E–01	5.93E–02	7.98E+00	4.66E+03	45.5 \pm 0.3
1200	0.641	12.184	3.65E–03	2.71E–01	8.48E–02	8.71E+00	2.39E+03	46.4 \pm 0.3
1300	0.689	8.010	2.44E–03	2.12E–01	8.65E–02	8.84E+00	3.62E+03	49.3 \pm 1.8
1400	0.944	9.873	3.03E–03	2.23E–01	8.72E–02	8.92E+00	2.95E+03	48.7 \pm 0.3
1500	1.000	10.730	3.42E–03	3.32E–01	9.29E–02	9.21E+00	2.69E+03	49.8 \pm 0.5
Integrated date = 46.9 \pm 0.3 Ma								
Plateau date = 46.5 \pm 0.3 Ma (700–1500 °C)								
J-value = 0.003415284 \pm 0.000018960								
<i>ST059A</i>								
600	0.009	65.363	6.86E–02	3.61E–01	1.07E–01	3.10E+01	4.52E+02	65.0 \pm 1.5
650	0.049	40.539	1.63E–02	9.03E–01	6.28E–02	1.17E+01	7.20E+02	42.4 \pm 1.6
700	0.062	21.156	5.54E–03	2.33E–01	2.67E–02	7.69E+00	1.39E+03	36.8 \pm 1.0
750	0.082	16.822	4.46E–03	1.05E–01	2.21E–02	7.82E+00	1.75E+03	39.5 \pm 0.8
800	0.183	17.920	4.85E–03	2.49E–01	2.29E–02	7.92E+00	1.63E+03	39.5 \pm 0.4

Table 2 (continued)

T(°C)	Cum. $^{39}\text{Ar}_\text{K}$ (%)	Atmos.	$^{36}\text{Ar}/^{39}\text{Ar}$	$^{37}\text{Ar}/^{39}\text{Ar}$	$^{38}\text{Ar}/^{39}\text{Ar}$	$^{40}\text{Ar}/^{39}\text{Ar}$	$^{40}\text{Ar}/^{36}\text{Ar}$	Date (Ma) $\pm 1\sigma$
<i>Southern province (Linzizong)</i>								
850	0.204	8.314	2.06E–03	1.76E–01	1.89E–02	7.19E+00	3.49E+03	40.0 \pm 0.6
900	0.235	6.131	1.55E–03	1.99E–01	1.87E–02	7.26E+00	4.68E+03	41.3 \pm 0.6
960	0.281	4.929	1.27E–03	1.74E–01	1.80E–02	7.37E+00	5.81E+03	42.5 \pm 0.4
1020	0.419	7.526	2.00E–03	1.56E–01	2.02E–02	7.74E+00	3.86E+03	43.4 \pm 0.3
1100	0.476	10.042	3.03E–03	9.09E–02	2.69E–02	8.87E+00	2.93E+03	48.3 \pm 0.3
1200	0.564	15.834	5.12E–03	1.04E–01	2.94E–02	9.54E+00	1.86E+03	48.7 \pm 0.4
1300	0.651	14.773	4.76E–03	6.81E–02	2.98E–02	9.52E+00	2.00E+03	49.2 \pm 0.3
1400	0.965	15.810	5.13E–03	1.07E–01	2.96E–02	9.56E+00	1.87E+03	48.8 \pm 0.3
1500	1.000	23.349	8.47E–03	1.41E–01	3.14E–02	1.07E+01	1.26E+03	49.7 \pm 0.3
Integrated date = 46.0 \pm 0.3 Ma								
Plateau date = 48.8 \pm 0.3 Ma (1100–500 °C)								
600	0.004	46.455	2.83E–02	3.69E–01	8.44E–02	1.80E+01	6.35E+02	58.2 \pm 4.5
650	0.014	30.458	1.07E–02	1.02E–01	4.23E–02	1.04E+01	9.71E+02	43.9 \pm 1.5
700	0.035	16.774	4.90E–03	1.20E–01	2.72E–02	8.61E+00	1.76E+03	43.5 \pm 0.5
750	0.113	9.952	2.88E–03	1.13E–01	2.39E–02	8.49E+00	2.95E+03	46.3 \pm 0.4
800	0.172	5.015	1.42E–03	9.53E–02	1.90E–02	8.24E+00	5.81E+03	47.4 \pm 0.4
850	0.247	3.661	1.03E–03	6.86E–02	1.81E–02	8.21E+00	7.96E+03	47.9 \pm 0.3
900	0.581	1.937	5.73E–04	1.38E–01	1.78E–02	8.23E+00	1.44E+04	48.9 \pm 0.9
960	0.607	5.984	1.77E–03	2.29E–01	1.92E–02	8.49E+00	4.79E+03	48.4 \pm 0.8
1020	0.747	3.918	1.17E–03	9.98E–02	2.04E–02	8.69E+00	7.40E+03	50.6 \pm 0.3
1100	0.766	8.675	2.88E–03	1.51E–01	3.69E–02	9.70E+00	3.37E+03	53.6 \pm 0.9
1200	0.788	8.554	3.03E–03	2.54E–01	4.51E–02	1.03E+01	3.39E+03	56.8 \pm 0.7
1300	0.808	9.670	3.46E–03	2.33E–01	4.16E–02	1.04E+01	3.01E+03	56.9 \pm 0.4
1400	0.848	11.150	4.04E–03	1.55E–01	4.36E–02	1.06E+01	2.63E+03	57.1 \pm 0.4
1500	0.868	17.438	6.71E–03	1.61E–01	4.63E–02	1.13E+01	1.69E+03	56.6 \pm 1.0
1600	1.000	18.733	7.51E–03	1.72E–01	4.65E–02	1.18E+01	1.57E+03	58.1 \pm 0.3
Integrated date = 50.8 \pm 0.4 Ma								
Plateau date = 48.7 \pm 0.5 Ma (750–1020 °C)								
600	0.010	77.907	1.20E–01	1.73E–02	2.15E–01	4.53E+01	3.80E+02	60.6 \pm 4.1
650	0.071	55.452	3.25E–02	9.73E–01	9.86E–02	1.72E+01	5.30E+02	46.5 \pm 1.8
700	0.080	7.920	2.47E–03	9.01E–01	4.92E–02	8.37E+00	3.40E+03	46.8 \pm 3.2
750	0.095	3.120	8.97E–04	8.65E–02	4.34E–02	8.32E+00	9.27E+03	48.8 \pm 3.0
800	0.220	20.901	6.59E–03	5.86E–01	4.73E–02	9.14E+00	1.39E+03	43.9 \pm 1.2
850	0.236	1.434	5.93E–04	8.27E–01	4.40E–02	7.91E+00	1.33E+04	47.3 \pm 3.4
900	0.257	2.480	8.09E–04	5.41E–01	5.52E–02	8.02E+00	9.92E+03	47.4 \pm 2.3
960	0.450	0.991	3.64E–04	3.64E–01	6.27E–02	8.11E+00	2.23E+04	48.6 \pm 0.4
1020	0.548	4.017	1.22E–03	3.01E–01	8.85E–02	8.43E+00	6.92E+03	49.0 \pm 0.4
1100	0.620	1.881	6.21E–04	3.05E–01	9.71E–02	8.56E+00	1.38E+04	50.9 \pm 0.7
1200	0.897	3.758	1.13E–03	1.35E–01	8.32E–02	8.65E+00	7.65E+03	50.4 \pm 0.3
1400	0.931	3.087	1.02E–03	1.94E–01	9.86E–02	9.30E+00	9.13E+03	54.5 \pm 1.1
1500	1.000	10.503	3.51E–03	3.42E–01	9.76E–02	9.67E+00	2.75E+03	52.4 \pm 0.7
Integrated date = 49.1 \pm 0.4 Ma								
Plateau date = 48.5 \pm 0.4 Ma (650–1200 °C)								
700	0.048	4.981	3.09E–03	2.45E+00	6.44E–02	1.47E+01	4.75E+03	93.9 \pm 2.1
750	0.111	10.015	4.29E–03	2.45E+00	4.04E–02	1.09E+01	2.53E+03	66.2 \pm 0.7
800	0.187	0.000	1.90E–04	2.47E+00	2.84E–02	8.03E+00	4.22E+04	54.6 \pm 2.1
850	0.268	0.000	2.33E–06	1.98E+00	2.21E–02	7.19E+00	3.09E+06	48.9 \pm 1.2
900	0.351	0.000	4.06E–04	1.72E+00	1.93E–02	6.98E+00	1.72E+04	47.5 \pm 0.9
960	0.440	0.000	2.28E–04	1.57E+00	2.22E–02	6.93E+00	3.03E+04	47.1 \pm 0.8
1020	0.578	0.357	4.63E–04	1.48E+00	2.47E–02	7.14E+00	1.54E+04	48.4 \pm 0.6
1100	0.744	18.630	6.14E–03	1.91E+00	3.70E–02	9.00E+00	1.47E+03	49.9 \pm 0.6
1200	0.884	14.587	1.11E–02	4.37E+00	9.17E–02	2.04E+01	1.83E+03	116.5 \pm 1.2
1300	0.924	18.873	3.82E–02	8.00E+00	2.36E–01	5.67E+01	1.48E+03	294.1 \pm 2.9
1400	0.947	20.492	4.46E–02	8.72E+00	2.39E–01	6.12E+01	1.37E+03	310.0 \pm 5.0
1500	1.000	22.153	5.71E–02	1.05E+01	3.01E–01	7.26E+01	1.27E+03	355.7 \pm 3.1
Integrated date = 96.1 \pm 0.9 Ma								
Plateau date = 49.3 \pm 0.6 Ma (800–1100 °C)								
600	0.006	72.537	5.46E–02	3.77E–01	6.32E–02	2.22E+01	4.07E+02	41.7 \pm 9.5
650	0.020	45.286	1.76E–02	2.73E–01	4.66E–02	1.15E+01	6.52E+02	42.8 \pm 2.2
700	0.046	23.449	6.76E–03	2.68E–01	5.02E–02	8.46E+00	1.25E+03	44.1 \pm 2.0
750	0.097	18.465	4.74E–03	3.62E–01	5.32E–02	7.47E+00	1.58E+03	41.5 \pm 0.5
800	0.164	11.100	2.82E–03	4.82E–01	5.60E–02	7.21E+00	2.56E+03	43.6 \pm 0.7
850	0.328	5.271	1.47E–03	1.11E+00	5.41E–02	6.68E+00	4.54E+03	43.1 \pm 0.5
900	0.488	5.744	1.67E–03	1.43E+00	4.79E–02	6.73E+00	4.04E+03	43.2 \pm 0.4
960	0.565	10.165	2.74E–03	1.45E+00	3.25E–02	6.91E+00	2.53E+03	42.3 \pm 0.4
1020	0.632	12.419	3.34E–03	1.08E+00	3.73E–02	7.32E+00	2.19E+03	43.6 \pm 1.0
1100	0.759	7.805	2.06E–03	4.47E–01	5.59E–02	7.40E+00	3.59E+03	46.4 \pm 0.7
1200	0.851	8.776	2.37E–03	4.66E–01	5.91E–02	7.62E+00	3.21E+03	47.3 \pm 0.8
1300	0.922	10.407	3.26E–03	1.01E+00	5.69E–02	8.56E+00	2.62E+03	52.1 \pm 0.7
1400	0.963	8.652	3.13E–03	1.10E+00	5.56E–02	9.75E+00	3.12E+03	60.4 \pm 0.9

(continued on next page)

Table 2 (continued)

T(°C)	Cum. $^{39}\text{Ar}_\text{K}$ (%)	Atmos.	$^{36}\text{Ar}/^{39}\text{Ar}$	$^{37}\text{Ar}/^{39}\text{Ar}$	$^{38}\text{Ar}/^{39}\text{Ar}$	$^{40}\text{Ar}/^{39}\text{Ar}$	$^{40}\text{Ar}/^{36}\text{Ar}$	Date (Ma) $\pm 1\sigma$
<i>Southern province (Linzizong)</i>								
1500	1.000	23.031	9.27E−03	1.99E+00	5.01E−02	1.13E+01	1.22E+03	58.9 \pm 0.9
Integrated date = 45.8 \pm 0.4 Ma						J-value = 0.003833268 \pm 0.000033185		
Plateau date = 44.0 \pm 0.4 Ma (600–1200 °C)								
600	0.027	0.000	2.55E−06	2.12E−01	1.67E−01	8.08E+00	3.17E+06	45.1 \pm 4.5
650	0.072	0.000	1.55E−06	1.84E−01	1.25E−01	7.91E+00	5.12E+06	44.2 \pm 3.3
700	0.130	0.000	1.18E−06	1.54E−01	9.29E−02	8.80E+00	7.43E+06	49.1 \pm 3.4
750	0.220	1.067	3.67E−04	1.31E−01	5.79E−02	9.26E+00	2.52E+04	51.1 \pm 2.5
800	0.334	0.429	1.68E−04	1.36E−01	4.84E−02	9.21E+00	5.48E+04	51.2 \pm 2.2
850	0.447	0.717	2.63E−04	1.84E−01	4.57E−02	8.92E+00	3.40E+04	49.5 \pm 1.9
900	0.544	4.689	1.45E−03	2.77E−01	3.51E−02	8.71E+00	6.02E+03	46.4 \pm 1.1
960	0.631	8.256	2.63E−03	3.21E−01	3.49E−02	9.15E+00	3.48E+03	46.9 \pm 1.0
1020	0.716	9.364	3.88E−03	3.14E−01	3.61E−02	1.20E+01	3.10E+03	60.6 \pm 1.1
1100	0.858	6.766	3.08E−03	2.03E−01	2.60E−02	1.33E+01	4.30E+03	68.7 \pm 1.2
1200	1.000	4.177	2.46E−03	4.74E−01	3.53E−02	1.66E+01	6.74E+03	87.9 \pm 1.5
Integrated date = 58.1 \pm 1.1 Ma						J-value = 0.003148017 \pm 0.000053046		
Plateau date = 48.6 \pm 1.1 Ma (600–960 °C)								
600	0.026	27.392	7.84E−03	1.59E−01	1.13E−01	8.44E+00	1.08E+03	34.3 \pm 5.5
650	0.072	23.049	5.77E−03	8.19E−02	6.37E−02	7.41E+00	1.28E+03	32.0 \pm 1.5
700	0.162	8.171	2.31E−03	4.32E−02	3.51E−02	8.34E+00	3.61E+03	42.8 \pm 1.9
750	0.315	5.461	1.68E−03	2.81E−02	2.44E−02	9.08E+00	5.41E+03	47.9 \pm 1.2
800	0.506	2.220	6.76E−04	2.48E−02	2.26E−02	8.94E+00	1.32E+04	48.8 \pm 1.1
850	0.681	3.381	1.03E−03	2.77E−02	2.16E−02	8.95E+00	8.71E+03	48.3 \pm 1.0
900	0.795	1.420	4.38E−04	3.67E−02	2.13E−02	8.95E+00	2.04E+04	49.3 \pm 0.9
960	0.862	6.860	2.06E−03	5.30E−02	2.49E−02	8.83E+00	4.29E+03	46.0 \pm 0.9
1020	0.911	1.322	4.05E−04	5.79E−02	2.72E−02	8.75E+00	2.16E+04	48.2 \pm 0.9
1100	0.956	5.490	1.65E−03	5.34E−02	2.68E−02	8.81E+00	5.36E+03	46.5 \pm 0.8
1200	1.000	0.000	1.09E−06	5.46E−02	2.55E−02	8.92E+00	8.15E+06	49.8 \pm 0.9
Integrated date = 46.7 \pm 0.8 Ma						J-value = 0.003148017 \pm 0.000053046		
Plateau date = 47.8 \pm 0.9 Ma (700–1200 °C)								
600	0.054	97.947	1.83E−02	4.01E−01	1.90E−01	5.52E+00	3.02E+02	0.6 \pm 3.7
650	0.096	92.190	2.09E−02	4.59E−01	1.81E−01	6.68E+00	3.20E+02	2.9 \pm 2.3
700	0.155	56.384	1.40E−02	5.78E−01	1.43E−01	7.29E+00	5.21E+02	17.9 \pm 1.4
750	0.241	18.165	5.19E−03	7.05E−01	1.28E−01	8.18E+00	1.58E+03	37.5 \pm 1.9
800	0.361	19.181	6.17E−03	7.30E−01	1.07E−01	9.25E+00	1.50E+03	41.9 \pm 1.0
850	0.515	11.207	3.68E−03	8.90E−01	1.01E−01	9.13E+00	2.48E+03	45.3 \pm 0.8
900	0.657	9.765	3.25E−03	1.12E+00	9.35E−02	9.01E+00	2.77E+03	45.5 \pm 0.9
960	0.754	9.699	3.33E−03	1.68E+00	8.06E−02	8.88E+00	2.66E+03	44.9 \pm 1.7
1020	0.818	18.938	6.27E−03	2.48E+00	6.39E−02	8.83E+00	1.41E+03	40.1 \pm 1.5
1100	0.881	10.553	4.11E−03	2.58E+00	8.26E−02	9.68E+00	2.36E+03	48.5 \pm 1.9
1200	1.000	3.447	1.67E−03	1.68E+00	1.38E−01	1.07E+01	6.39E+03	57.6 \pm 1.1
Integrated date = 39.8 \pm 0.8 Ma						J-value = 0.003148017 \pm 0.000053046		
Plateau date = 43.2 \pm 0.8 Ma (750–1020 °C)								
600	0.070	34.144	1.11E−02	1.35E+00	5.09E−02	9.35E+00	8.41E+02	37.5 \pm 1.4
650	0.121	0.000	1.42E−06	2.97E−01	4.79E−02	8.15E+00	5.72E+06	49.3 \pm 0.4
700	0.254	0.000	5.51E−07	1.95E−01	2.75E−02	8.59E+00	1.56E+07	52.0 \pm 0.5
750	0.507	3.791	1.20E−03	1.01E−01	1.85E−02	9.15E+00	7.65E+03	53.3 \pm 0.4
800	0.733	6.341	2.08E−03	1.98E−01	1.93E−02	9.48E+00	4.56E+03	53.7 \pm 0.8
850	0.845	6.318	2.08E−03	4.73E−01	2.41E−02	9.20E+00	4.42E+03	52.2 \pm 0.9
900	0.902	9.154	2.92E−03	2.42E+00	6.06E−02	7.45E+00	2.56E+03	41.1 \pm 2.4
960	0.922	14.553	4.74E−03	1.60E+00	5.45E−02	8.83E+00	1.86E+03	45.8 \pm 1.5
1020	0.945	25.206	9.66E−03	9.80E−01	4.78E−02	1.11E+01	1.15E+03	50.2 \pm 1.4
1100	0.966	42.172	2.12E−02	1.28E+00	7.53E−02	1.47E+01	6.91E+02	51.4 \pm 2.3
1200	0.976	43.915	4.21E−02	1.89E+00	1.12E−01	2.81E+01	6.66E+02	94.5 \pm 2.0
1300	0.984	22.932	4.45E−02	8.69E−01	1.45E−01	5.71E+01	1.28E+03	252.8 \pm 5.0
1400	0.990	28.150	6.17E−02	1.28E+00	1.68E−01	6.44E+01	1.05E+03	264.9 \pm 5.6
1500	1.000	30.322	8.41E−02	1.56E−01	1.71E−01	8.19E+01	9.74E+02	321.3 \pm 2.9
Integrated date = 57.1 \pm 0.4 Ma						J-value = 0.003415284 \pm 0.000018960		
Plateau date = 53.0 \pm 0.4 Ma (700–850 °C)								
600	0.022	23.678	2.09E−02	2.13E+00	8.31E−02	2.55E+01	1.22E+03	107.1 \pm 3.0
650	0.079	37.491	1.77E−02	2.40E+00	9.25E−02	1.35E+01	7.63E+02	47.2 \pm 3.8
700	0.119	28.809	1.15E−02	1.52E+00	5.75E−02	1.14E+01	9.94E+02	45.6 \pm 1.0
750	0.159	16.198	5.50E−03	1.29E+00	4.19E−02	9.46E+00	1.72E+03	44.4 \pm 1.4
800	0.210	16.057	5.22E−03	1.23E+00	3.68E−02	9.06E+00	1.74E+03	42.6 \pm 1.5
850	0.281	11.962	3.95E−03	1.19E+00	3.49E−02	9.03E+00	2.29E+03	44.5 \pm 1.4
900	0.339	9.754	3.15E−03	1.20E+00	3.87E−02	8.65E+00	2.74E+03	43.7 \pm 1.4
960	0.387	15.534	5.15E−03	1.19E+00	4.17E−02	9.26E+00	1.80E+03	43.8 \pm 1.7
1020	0.546	13.562	4.98E−03	1.53E+00	5.45E−02	1.00E+01	2.01E+03	48.4 \pm 0.9
1100	0.605	12.555	5.73E−03	1.72E+00	6.36E−02	1.25E+01	2.18E+03	60.9 \pm 1.4
1200	1.000	6.737	4.00E−03	1.36E+00	5.12E−02	1.61E+01	4.01E+03	83.1 \pm 1.4
Integrated date = 62.8 \pm 1.1 Ma						J-value = 0.003148017 \pm 0.000053046		
Plateau date = 45.7 \pm 0.9 Ma (650–1020 °C)								

Table 2 (continued)

T(°C)	Cum. $^{39}\text{Ar}_\text{K}$ (%)	Atmos.	$^{36}\text{Ar}/^{39}\text{Ar}$	$^{37}\text{Ar}/^{39}\text{Ar}$	$^{38}\text{Ar}/^{39}\text{Ar}$	$^{40}\text{Ar}/^{39}\text{Ar}$	$^{40}\text{Ar}/^{36}\text{Ar}$	Date (Ma) $\pm 1\sigma$
<i>Southern province (Linzizong)</i>								
600	0.014	70.392	4.47E−02	2.45E−01	1.26E−01	1.88E+01	4.20E+02	31.2 \pm 3.6
650	0.047	0.000	2.01E−06	1.93E−01	1.52E−01	8.15E+00	4.07E+06	45.6 \pm 7.1
700	0.099	0.000	1.26E−06	1.49E−01	1.18E−01	7.33E+00	5.80E+06	41.0 \pm 3.6
750	0.192	0.000	7.06E−07	1.14E−01	8.22E−02	8.68E+00	1.23E+07	48.5 \pm 2.8
800	0.309	0.000	5.67E−07	1.06E−01	7.62E−02	8.60E+00	1.52E+07	48.1 \pm 3.3
850	0.430	3.410	1.07E−03	1.12E−01	7.06E−02	9.02E+00	8.46E+03	48.7 \pm 2.1
900	0.551	5.927	1.82E−03	1.09E−01	5.87E−02	8.94E+00	4.93E+03	47.0 \pm 2.3
960	0.703	5.330	1.68E−03	9.24E−02	4.53E−02	9.21E+00	5.48E+03	48.7 \pm 2.1
1020	0.867	3.740	1.21E−03	7.67E−02	4.02E−02	9.43E+00	7.80E+03	50.7 \pm 1.5
1100	0.955	9.976	3.16E−03	1.26E−01	5.96E−02	9.29E+00	2.94E+03	46.7 \pm 1.4
1200	1.000	25.835	8.85E−03	1.65E−01	8.17E−02	1.01E+01	1.14E+03	42.0 \pm 1.0
Integrated date = 47.5 \pm 1.1 Ma								
Plateau date = 47.7 \pm 1.1 Ma (650–1200 °C)								
T038F								
600	0.014	51.104	1.23E−02	3.17E+00	9.39E−02	6.68E+00	5.43E+02	18.4 \pm 1.8
650	0.042	32.914	8.07E−03	2.53E+00	9.32E−02	6.69E+00	8.30E+02	25.3 \pm 0.7
700	0.099	7.415	2.39E−03	1.69E+00	9.90E−02	7.82E+00	3.28E+03	40.6 \pm 1.7
750	0.209	6.941	2.35E−03	1.23E+00	1.10E−01	8.69E+00	3.70E+03	45.3 \pm 0.9
840	0.405	7.634	2.62E−03	7.38E−01	1.24E−01	9.44E+00	3.60E+03	48.7 \pm 0.8
900	0.630	5.702	2.01E−03	1.27E+00	1.19E−01	8.77E+00	4.36E+03	46.3 \pm 0.8
960	0.697	1.061	8.43E−04	2.21E+00	1.04E−01	7.81E+00	9.26E+03	43.2 \pm 0.8
1020	0.754	5.262	1.96E−03	1.99E+00	1.08E−01	8.16E+00	4.17E+03	43.3 \pm 0.8
1100	0.828	11.461	3.76E−03	1.31E+00	1.17E−01	8.87E+00	2.36E+03	44.0 \pm 0.8
1200	0.897	11.840	3.94E−03	1.50E+00	1.07E−01	8.92E+00	2.26E+03	44.0 \pm 0.8
1300	0.938	13.616	4.40E−03	2.08E+00	1.11E−01	8.43E+00	1.92E+03	40.8 \pm 1.0
1400	0.968	5.477	2.15E−03	2.48E+00	1.20E−01	8.22E+00	3.82E+03	43.5 \pm 0.8
1600	1.000	15.026	5.08E−03	2.47E+00	1.26E−01	8.78E+00	1.73E+03	41.8 \pm 1.5
Integrated date = 44.2 \pm 0.7 Ma								
Plateau date = 45.1 \pm 0.8 Ma (700–1600 °C)								
T038G								
600	0.014	16.674	1.43E−03	2.13E+00	1.76E−01	1.60E+00	1.12E+03	8.1 \pm 0.5
650	0.342	36.515	6.06E−03	1.42E+00	1.22E−01	4.64E+00	7.66E+02	18.0 \pm 0.9
700	0.426	27.131	5.29E−03	1.25E+00	1.04E−01	5.44E+00	1.03E+03	24.2 \pm 0.8
750	0.479	12.067	3.04E−03	8.34E−01	6.41E−02	6.95E+00	2.29E+03	37.1 \pm 0.6
800	0.499	0.000	1.44E−06	9.69E−01	7.05E−02	6.21E+00	4.30E+06	37.7 \pm 2.6
850	0.541	11.575	3.49E−03	5.12E−01	3.74E−02	8.60E+00	2.47E+03	46.1 \pm 0.4
900	0.613	14.557	4.60E−03	4.28E−01	3.55E−02	9.14E+00	1.99E+03	47.3 \pm 0.4
960	0.630	16.013	5.12E−03	5.75E−01	5.29E−02	9.21E+00	1.80E+03	46.9 \pm 1.0
1020	0.735	27.153	9.97E−03	4.94E−01	5.72E−02	1.07E+01	1.08E+03	47.5 \pm 1.0
1100	0.785	34.762	1.49E−02	2.77E−01	4.60E−02	1.26E+01	8.48E+02	50.0 \pm 0.5
1200	0.933	43.455	2.20E−02	2.12E−01	4.27E−02	1.49E+01	6.80E+02	51.2 \pm 0.4
1300	1.000	55.753	3.47E−02	2.96E−01	4.79E−02	1.84E+01	5.30E+02	49.3 \pm 0.5
Integrated date = 33.0 \pm 0.5 Ma								
Plateau date = 48.9 \pm 0.4 Ma (850–1300 °C)								
T155								
600	0.250	37.084	8.42E−03	8.08E−01	1.85E−02	6.57E+00	7.81E+02	28.3 \pm 0.9
650	0.342	20.096	4.93E−03	6.95E−01	1.74E−02	7.02E+00	1.42E+03	38.2 \pm 0.8
700	0.426	13.132	3.72E−03	7.44E−01	1.62E−02	7.96E+00	2.14E+03	47.1 \pm 0.6
750	0.235	7.122	2.22E−03	8.53E−01	1.50E−02	8.34E+00	3.76E+03	52.7 \pm 0.7
800	0.307	6.053	1.97E−03	8.64E−01	1.42E−02	8.56E+00	4.35E+03	54.6 \pm 0.7
850	0.381	6.714	2.24E−03	9.75E−01	1.41E−02	8.79E+00	3.93E+03	55.7 \pm 0.5
900	0.427	8.140	2.69E−03	9.80E−01	1.49E−02	8.89E+00	3.30E+03	55.5 \pm 0.7
960	0.494	13.003	4.29E−03	1.09E+00	1.47E−02	9.14E+00	2.13E+03	54.0 \pm 0.9
1020	0.587	8.695	2.78E−03	9.13E−01	1.49E−02	8.67E+00	3.12E+03	53.8 \pm 0.6
1100	0.709	8.227	2.59E−03	9.40E−01	1.53E−02	8.47E+00	3.27E+03	52.8 \pm 0.6
1200	0.810	11.946	4.08E−03	1.88E+00	1.60E−02	8.92E+00	2.19E+03	53.4 \pm 0.6
1300	0.972	16.489	6.18E−03	3.57E+00	1.68E−02	9.46E+00	1.53E+03	53.8 \pm 0.6
1400	0.994	40.222	2.52E−02	1.74E+01	2.21E−02	1.53E+01	6.06E+02	62.6 \pm 2.2
1500	1.000	61.731	4.44E−02	7.06E+00	3.10E−02	2.04E+01	4.60E+02	53.4 \pm 2.2
Integrated date = 51.6 \pm 0.5 Ma								
Plateau date = 53.9 \pm 0.5 Ma (750–1300 °C)								
T151								
600	0.045	34.794	1.30E−02	5.97E−01	4.33E−02	1.09E+01	8.42E+02	43.2 \pm 1.0
650	0.091	3.473	1.26E−03	3.14E−01	3.16E−02	1.00E+01	7.99E+03	58.5 \pm 0.9
700	0.225	1.766	7.08E−04	4.11E−01	2.70E−02	1.01E+01	1.43E+04	60.1 \pm 1.1
750	0.411	1.003	3.89E−04	1.69E−01	2.82E−02	1.02E+01	2.63E+04	61.1 \pm 0.9
800	0.579	1.923	7.09E−04	1.36E−01	2.95E−02	1.04E+01	1.47E+04	61.5 \pm 0.7
850	0.706	1.385	5.04E−04	1.24E−01	2.56E−02	1.01E+01	2.01E+04	60.2 \pm 0.5
900	0.779	1.706	6.07E−04	1.69E−01	2.54E−02	9.80E+00	1.61E+04	58.3 \pm 0.5
960	0.834	3.205	1.13E−03	2.96E−01	3.73E−02	9.73E+00	8.63E+03	57.0 \pm 0.6
1020	0.875	5.324	1.86E−03	4.29E−01	3.77E−02	9.76E+00	5.24E+03	55.9 \pm 0.8
1100	0.914	4.143	1.42E−03	1.27E−01	2.38E−02	9.95E+00	6.99E+03	57.7 \pm 0.6
1200	0.942	11.448	4.26E−03	1.13E−01	2.37E−02	1.10E+01	2.57E+03	58.6 \pm 0.6
1300	0.954	17.883	7.26E−03	2.20E−01	2.74E−02	1.19E+01	1.64E+03	59.3 \pm 1.8

(continued on next page)

Table 2 (continued)

T(°C)	Cum. $^{39}\text{Ar}_\text{K}$ (%)	Atmos.	$^{36}\text{Ar}/^{39}\text{Ar}$	$^{37}\text{Ar}/^{39}\text{Ar}$	$^{38}\text{Ar}/^{39}\text{Ar}$	$^{40}\text{Ar}/^{39}\text{Ar}$	$^{40}\text{Ar}/^{36}\text{Ar}$	Date (Ma) $\pm 1\sigma$
<i>Southern province (Linzizong)</i>								
1400	0.967	15.615	6.36E−03	1.93E−01	2.59E−02	1.20E+01	1.88E+03	61.1 \pm 0.8
1500	0.981	13.826	5.61E−03	5.70E−02	2.53E−02	1.20E+01	2.14E+03	62.4 \pm 0.9
1600	1.000	18.851	8.06E−03	2.38E−01	2.75E−02	1.26E+01	1.56E+03	61.6 \pm 1.2
Integrated date = 59.5 \pm 0.4 Ma								
Plateau date = 59.9 \pm 0.4 Ma (650–1600 °C)								
<i>Northern province</i>								
600	0.084	86.221	1.90E−01	8.18E−01	7.82E−02	6.52E+01	3.43E+02	54.5 \pm 4.2
650	0.212	48.905	6.04E−02	7.48E−01	4.05E−02	3.64E+01	6.03E+02	111.0 \pm 2.0
700	0.484	41.466	4.50E−02	1.06E+00	4.45E−02	3.19E+01	7.09E+02	111.6 \pm 2.6
750	0.647	33.156	3.19E−02	1.00E+00	3.94E−02	2.82E+01	8.85E+02	112.6 \pm 1.5
800	0.756	26.904	2.43E−02	1.51E+00	4.41E−02	2.63E+01	1.08E+03	114.8 \pm 6.1
850	0.835	32.614	2.64E−02	2.08E+00	6.46E−02	2.35E+01	8.89E+02	94.8 \pm 2.4
900	0.875	42.971	3.18E−02	3.97E+00	8.35E−02	2.12E+01	6.67E+02	73.1 \pm 10.6
960	0.908	26.818	1.93E−02	4.90E+00	9.80E−02	1.99E+01	1.03E+03	87.8 \pm 6.8
1020	0.945	56.720	5.89E−02	4.63E+00	1.09E−01	3.01E+01	5.11E+02	78.7 \pm 6.7
1100	0.974	68.045	6.84E−02	4.09E+00	9.17E−02	2.93E+01	4.28E+02	56.8 \pm 10.3
1200	1.000	76.449	1.18E−01	5.04E+00	1.53E−01	4.50E+01	3.83E+02	64.3 \pm 11.6
Integrated date = 99.7 \pm 1.4 Ma								
Plateau date = 112.3 \pm 1.6 Ma (650–800 °C)								
600	0.018	3.055	1.35E−03	3.47E−02	1.37E−02	1.30E+01	9.63E+03	75.9 \pm 0.9
650	0.066	0.465	2.26E−04	3.36E−02	1.31E−02	1.38E+01	6.13E+04	82.8 \pm 1.0
700	0.354	0.978	4.84E−04	3.51E−02	1.36E−02	1.44E+01	2.97E+04	85.6 \pm 0.6
750	0.438	2.670	1.36E−03	2.20E−02	1.33E−02	1.50E+01	1.10E+04	87.4 \pm 0.5
800	0.673	1.756	8.73E−04	2.50E−02	1.35E−02	1.46E+01	1.67E+04	86.2 \pm 0.5
850	0.711	2.197	1.00E−03	2.39E−02	1.32E−02	1.35E+01	1.34E+04	79.2 \pm 0.9
900	0.794	2.181	9.84E−04	4.24E−02	1.43E−02	1.32E+01	1.34E+04	77.7 \pm 0.5
960	0.821	4.116	1.81E−03	3.98E−03	1.43E−02	1.30E+01	7.19E+03	75.1 \pm 0.6
1020	0.848	5.917	2.58E−03	3.57E−02	1.44E−02	1.29E+01	4.99E+03	72.9 \pm 0.7
1100	0.935	4.470	1.97E−03	2.44E−02	1.49E−02	1.30E+01	6.60E+03	74.8 \pm 0.5
1200	0.950	8.909	4.19E−03	6.03E−02	1.52E−02	1.39E+01	3.31E+03	76.1 \pm 0.9
1300	0.969	0.000	2.09E−06	6.01E−02	1.56E−02	1.52E+01	7.27E+06	91.0 \pm 0.9
1400	0.986	9.886	5.27E−03	6.71E−02	1.82E−02	1.57E+01	2.99E+03	85.1 \pm 1.5
1500	1.000	8.768	4.84E−03	1.42E−01	1.90E−02	1.62E+01	3.35E+03	88.8 \pm 1.5
Integrated date = 83.1 \pm 0.5 Ma								
Plateau date = 85.8 \pm 0.5 Ma (650–800 °C)								
600	0.031	52.118	5.36E−02	1.00E+00	3.21E−02	3.03E+01	5.65E+02	87.1 \pm 2.7
650	0.056	42.753	4.32E−02	1.12E+00	2.88E−02	2.97E+01	6.87E+02	101.8 \pm 5.4
700	0.098	40.716	3.99E−02	2.12E+00	2.46E−02	2.86E+01	7.17E+02	101.5 \pm 4.1
750	0.169	35.632	3.58E−02	1.82E+00	2.85E−02	2.93E+01	8.19E+02	112.6 \pm 5.9
800	0.341	31.406	2.80E−02	2.02E+00	3.22E−02	2.59E+01	9.25E+02	106.1 \pm 1.7
850	0.397	29.081	2.46E−02	2.88E+00	2.44E−02	2.43E+01	9.87E+02	103.2 \pm 2.6
900	0.442	19.323	1.53E−02	2.50E+00	1.89E−02	2.25E+01	1.47E+03	108.5 \pm 5.1
960	0.644	20.899	1.62E−02	2.79E+00	3.48E−02	2.19E+01	1.35E+03	103.9 \pm 1.5
1020	0.676	39.763	2.92E−02	4.29E+00	3.31E−02	2.09E+01	7.16E+02	76.1 \pm 4.5
1100	0.719	32.050	2.62E−02	5.27E+00	4.37E−02	2.29E+01	8.76E+02	93.7 \pm 6.7
1200	0.850	19.114	1.77E−02	5.98E+00	5.09E−02	2.51E+01	1.42E+03	121.0 \pm 1.6
1300	0.870	48.558	4.58E−02	6.69E+00	5.93E−02	2.69E+01	5.87E+02	83.5 \pm 6.9
1400	0.931	39.207	3.93E−02	6.94E+00	5.35E−02	2.83E+01	7.21E+02	103.4 \pm 3.0
1500	1.000	28.530	2.95E−02	6.05E+00	5.82E−02	2.90E+01	9.83E+02	123.6 \pm 3.3
Integrated date = 106.3 \pm 1.0 Ma								
Plateau date = 105.6 \pm 1.2 Ma (650–960 °C)								
600	0.024	48.372	2.27E−02	5.67E−01	5.81E−02	1.38E+01	6.08E+02	43.4 \pm 0.9
650	0.098	14.337	5.06E−03	6.90E−01	4.06E−02	1.01E+01	2.00E+03	52.4 \pm 1.2
700	0.145	3.183	1.20E−03	1.41E−06	2.52E−02	1.11E+01	9.31E+03	65.1 \pm 0.7
750	0.228	4.367	1.84E−03	8.95E−02	2.39E−02	1.23E+01	6.70E+03	70.9 \pm 0.6
800	0.370	8.370	3.74E−03	5.00E−01	3.04E−02	1.28E+01	3.42E+03	70.7 \pm 0.7
850	0.435	9.469	4.36E−03	1.30E−01	1.94E−02	1.35E+01	3.10E+03	73.8 \pm 0.9
900	0.480	6.565	2.89E−03	1.89E−01	1.80E−02	1.28E+01	4.44E+03	72.1 \pm 0.8
960	0.537	4.180	1.79E−03	1.66E−01	1.66E−02	1.24E+01	6.92E+03	71.4 \pm 0.5
1020	0.604	2.940	1.27E−03	2.05E−01	1.57E−02	1.23E+01	9.66E+03	71.9 \pm 0.5
1100	0.729	1.570	6.96E−04	2.82E−01	1.57E−02	1.18E+01	1.69E+04	69.9 \pm 0.5
1200	0.826	3.471	1.51E−03	3.39E−01	2.04E−02	1.21E+01	8.04E+03	70.6 \pm 0.5
1300	0.894	13.374	6.62E−03	3.83E−01	6.63E−02	1.44E+01	2.18E+03	75.3 \pm 0.5
1400	0.949	25.566	1.46E−02	4.46E−01	7.78E−02	1.68E+01	1.15E+03	75.4 \pm 0.8
1500	1.000	24.625	1.48E−02	4.41E−01	6.70E−02	1.77E+01	1.19E+03	80.1 \pm 0.6
Integrated date = 69.8 \pm 0.4 Ma								
Plateau date = 71.1 \pm 0.4 Ma (750–1200 °C)								
600	0.106	7.566	4.67E−03	6.19E−02	1.65E−02	1.82E+01	3.90E+03	100.6 \pm 0.7
650	0.146	1.016	6.39E−04	6.03E−02	1.35E−02	1.82E+01	2.84E+04	107.4 \pm 0.7
700	0.286	0.764	4.79E−04	1.65E−02	1.28E−02	1.84E+01	3.84E+04	109.0 \pm 0.6

Table 2 (continued)

T(°C)	Cum. $^{39}\text{Ar}_\text{K}$ (%)	Atmos.	$^{36}\text{Ar}/^{39}\text{Ar}$	$^{37}\text{Ar}/^{39}\text{Ar}$	$^{38}\text{Ar}/^{39}\text{Ar}$	$^{40}\text{Ar}/^{39}\text{Ar}$	$^{40}\text{Ar}/^{36}\text{Ar}$	Date (Ma) $\pm 1\sigma$
<i>Northern province</i>								
750	0.534	1.052	6.67E–04	1.24E–02	1.31E–02	1.87E + 01	2.80E + 04	110.2 \pm 0.6
800	0.619	0.873	5.54E–04	8.83E–03	1.33E–02	1.87E + 01	3.38E + 04	110.5 \pm 0.7
900	0.635	2.816	1.78E–03	7.69E–02	1.54E–02	1.85E + 01	1.04E + 04	107.5 \pm 0.9
960	0.650	0.752	5.04E–04	1.35E–01	1.57E–02	1.85E + 01	3.67E + 04	109.6 \pm 0.9
1020	0.696	1.204	7.79E–04	6.81E–02	1.42E–02	1.87E + 01	2.40E + 04	110.3 \pm 0.8
1100	0.717	0.691	4.60E–04	8.38E–02	1.64E–02	1.88E + 01	4.09E + 04	111.3 \pm 1.4
1200	0.751	0.969	6.33E–04	4.41E–02	1.49E–02	1.90E + 01	3.00E + 04	112.1 \pm 0.8
1300	0.792	2.032	1.32E–03	4.28E–02	1.47E–02	1.91E + 01	1.44E + 04	111.6 \pm 0.8
1400	0.831	1.859	1.23E–03	5.84E–02	1.56E–02	1.93E + 01	1.57E + 04	113.0 \pm 0.9
1500	1.000	4.180	2.77E–03	7.04E–02	1.61E–02	1.95E + 01	7.03E + 03	111.4 \pm 0.7
Integrated date = 109.4 \pm 0.6 Ma								J-value = 0.003415284 \pm 0.000018960
Plateau date = 110.4 \pm 0.6 Ma (650–500 °C)								
<i>Sangri Group</i>								
600	0.103	18.255	1.01E–02	3.49E–01	2.37E–02	1.62E + 01	1.61E + 03	89.4 \pm 1.8
650	0.267	8.400	4.21E–03	1.68E–01	1.53E–02	1.47E + 01	3.49E + 03	90.6 \pm 0.9
700	0.495	3.451	1.81E–03	1.03E–01	1.36E–02	1.53E + 01	8.46E + 03	99.0 \pm 0.9
750	0.679	3.875	1.99E–03	8.72E–02	1.35E–02	1.51E + 01	7.56E + 03	97.2 \pm 1.3
800	0.802	1.942	1.00E–03	9.87E–02	1.38E–02	1.49E + 01	1.49E + 04	97.9 \pm 1.5
850	0.870	2.455	1.26E–03	1.62E–01	1.38E–02	1.47E + 01	1.17E + 04	96.2 \pm 2.2
900	0.919	3.008	1.67E–03	7.59E–01	1.49E–02	1.46E + 01	8.70E + 03	94.9 \pm 3.8
960	0.959	9.491	5.34E–03	2.08E + 00	2.27E–02	1.50E + 01	2.81E + 03	91.6 \pm 2.8
1020	0.973	16.841	1.27E–02	5.28E + 00	2.27E–02	1.99E + 01	1.57E + 03	111.4 \pm 9.7
1100	0.987	43.139	4.58E–02	6.58E + 00	5.84E–02	3.02E + 01	6.61E + 02	115.4 \pm 14.2
1200	1.000	40.167	8.05E–02	4.74E + 00	1.71E–01	5.84E + 01	7.25E + 02	227.2 \pm 7.0
Integrated date = 97.7 \pm 1.0 Ma								J-value = 0.003833268 \pm 0.000033185
Plateau date = 97.3 \pm 1.0 Ma (700–960 °C)								
600	0.013	31.933	2.20E–02	2.17E–01	6.58E–02	2.03E + 01	9.24E + 02	79.9 \pm 1.4
650	0.035	23.786	1.19E–02	1.42E–01	4.60E–02	1.47E + 01	1.24E + 03	65.0 \pm 1.9
700	0.074	26.448	1.15E–02	1.44E–01	4.15E–02	1.28E + 01	1.12E + 03	54.7 \pm 1.3
750	0.144	14.461	5.89E–03	1.22E–01	3.66E–02	1.20E + 01	2.04E + 03	59.5 \pm 0.7
800	0.243	5.689	2.51E–03	8.97E–02	2.96E–02	1.30E + 01	5.16E + 03	70.7 \pm 0.7
850	0.373	5.070	2.51E–03	6.17E–02	2.36E–02	1.46E + 01	5.80E + 03	79.7 \pm 0.6
900	0.531	3.642	1.95E–03	4.86E–02	2.25E–02	1.58E + 01	8.08E + 03	87.6 \pm 0.7
960	0.695	8.586	4.84E–03	4.36E–02	2.08E–02	1.66E + 01	3.44E + 03	87.6 \pm 0.9
1020	0.807	5.314	2.90E–03	7.28E–02	2.79E–02	1.60E + 01	5.54E + 03	87.5 \pm 0.7
1100	0.860	3.706	1.96E–03	9.96E–02	3.55E–02	1.54E + 01	7.89E + 03	85.6 \pm 1.1
1200	0.932	8.684	4.86E–03	1.13E–01	3.49E–02	1.65E + 01	3.39E + 03	86.6 \pm 0.9
1300	0.960	14.213	1.07E–02	1.93E–01	4.56E–02	2.21E + 01	2.07E + 03	108.7 \pm 1.6
1400	0.978	16.486	1.52E–02	1.87E–01	5.71E–02	2.73E + 01	1.79E + 03	129.7 \pm 1.4
1600	1.000	13.669	1.97E–02	2.41E–01	5.72E–02	4.26E + 01	2.16E + 03	205.0 \pm 2.2
Integrated date = 84.9 \pm 0.6 Ma								J-value = 0.003276164 \pm 0.000023240
Plateau date = 87.2 \pm 0.7 Ma (900–1200 °C)								

coupled with depletions in the high field strength elements (HFSE; e.g., Nb, Ta and Ti), similar to arc-lavas from the active continental margins along the circum-Pacific subduction zone (Tatsumi and Eggers, 1995). Paleogene volcanic rocks from the southern province, furthermore, show major compositional variations manifested by the occurrence of a shoshonitic suite in the Linzhou Basin and a low-K or tholeiitic suite (Fig. 5a). The latter suite of volcanic rocks, widespread in Xigaze, Nanmulin, Majiang and Lhasa areas (Fig. 1), is marked with possessing lower concentrations of incompatible trace elements, e.g., La \approx 7–10 ppm for basaltic rocks (Table 4), and thus less enriched LREE patterns than those of the associated calc-alkaline and shoshonitic suites of rocks (Fig. 5b).

5. Discussion

5.1. Age and extent of the Linzizong volcanism

Our new results and published age data (Fig. 4) suggest two discrete volcanic provinces in the Lhasa terrane. These are (1) the northern province active from ca. 112 to 70 Ma in the Cretaceous and (2) the southern province that comprises the Sangri Group aged ca. 90 Ma and the “real” Linzizong volcanic successions from ca. 69 to 43 Ma. Note that age data for the former include five analyses by this study (Figs. 1 and 2) and two others (dated ca. 111 and 74 Ma)

by Coulon et al. (1986); and all these Cretaceous samples were recovered from “the northern province”, i.e., the yellow-colored areas in Fig. 1, of the Linzizong volcanic successions mapped by Yin and Harrison (2000). Hence, these authors overmeasured the areal extent of the Linzizong successions, which, based on the above age constraints, should be confined to the southern part of the Lhasa terrane. Most of the yellow-colored areas should, instead, be included into Cretaceous volcano-sedimentary sequences or the Zenong Group in the middle and northern parts of the Gangdese belt (cf. Kapp et al., 2007b; Zhu et al., 2009). The Linzizong volcanic successions are distributed from Jinda in the east to Coqin in the west and westward in comparison to the Shiduo Group in the Ali area (Mo et al., 2003) and volcanic rocks near Jarga in SW Tibet (Miller et al., 2000).

Using zircon U-Pb method, He et al. (2007) reported the oldest age (68.7 ± 2.4 Ma) for a rhyolite at the base of the Linzizong successions. From corresponding sections in the nearby regions, however, Lee et al. (2007) reported a younger zircon U-Pb age of 62.5 ± 1.1 Ma for a rhyolitic tuff and Mo et al. (2003) reported a plagioclase $^{40}\text{Ar}/^{39}\text{Ar}$ age of 64.5 ± 0.8 Ma for an andesitic block (Table 3). Although precise onset timing of the Linzizong volcanism remains debatable and there is thermochronological evidence showing that some volcanic rocks were buried during the Paleogene and could have undergone argon loss (He et al., 2007), we conclude that the Linzizong successions

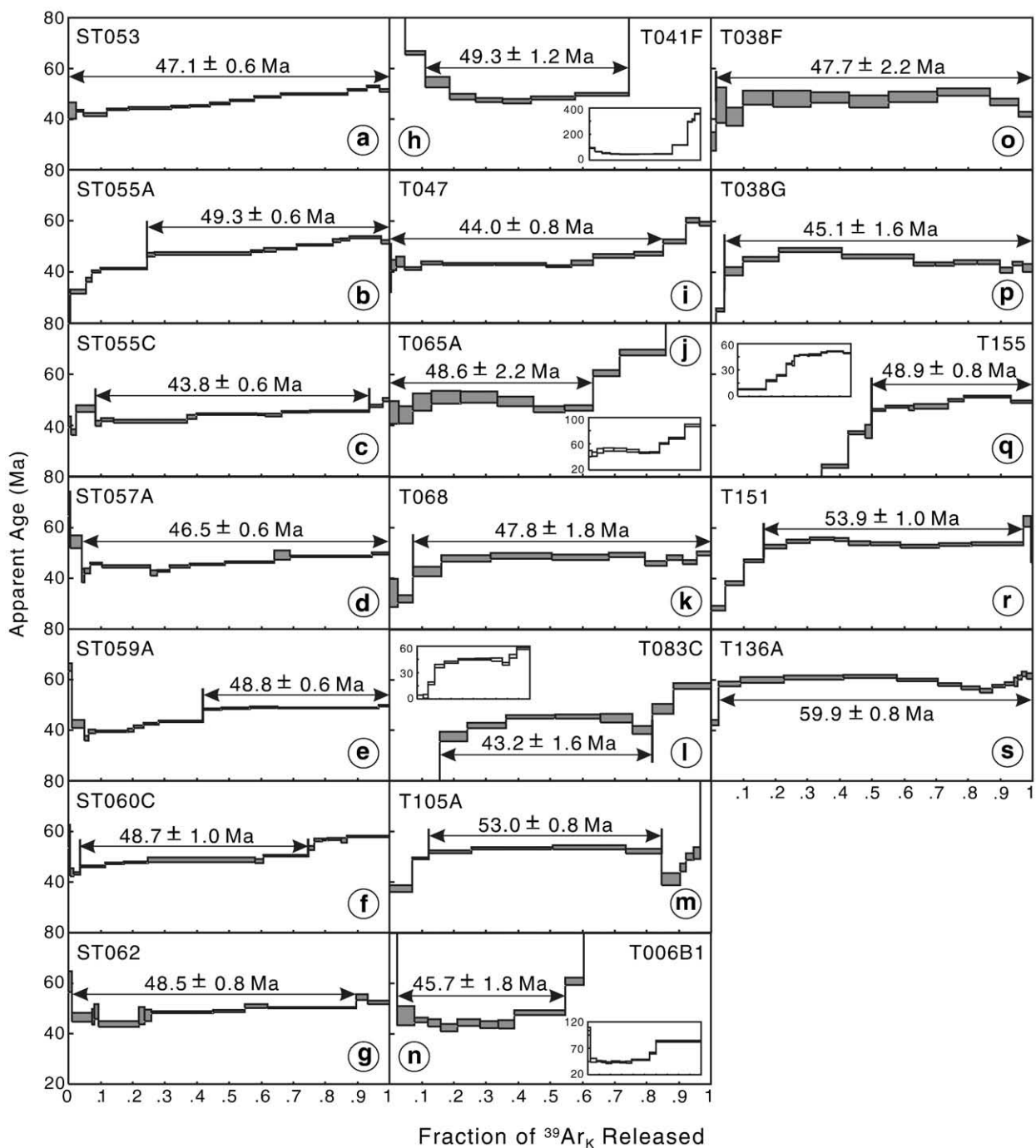


Fig. 2. Age spectra of volcanic rocks from the southern province. Plateau ages with 2σ analytical errors were calculated using the steps between arrows.

erupted during ca. 69–43 Ma (Fig. 4c). This duration is in good accordance with age results obtained for the Gangdese batholith, on which Wen et al. (2008) recently carried out a detailed zircon U-Pb geochronological study suggesting two distinct intrusive stages from ca. 103 to 80 Ma and from ca. 68 to 43 Ma, respectively, with a magmatic gap between ca. 80 and 68 Ma.

5.2. Southward volcanic migration and intensification

The age data, moreover, suggest southward migration (Fig. 4; b and c) and intensification of volcanic activity (Fig. 4c) in the Lhasa terrane. Eruptions during Cretaceous time appear to have been

widespread, occurring in both the northern and southern provinces. By contrast, in the Paleogene, volcanism became spatially confined and more intense in the south. The intensification is best manifested by the volcanic culmination or “flare-up” record around 50 Ma observed from the Linzizong successions. A coeval intrusive peak has also been identified in the Gangdese batholith (Wen et al., 2008). Such a magmatic flare-up and continued activities, lasting until ca. 45 Ma (Fig. 4 and Table 3), resulted in thick piles (>2000 m) of volcanic sequences in localities, e.g., the Linzhou Basin (Dong et al., 2005; He et al., 2007; Mo et al., 2008), and the major component of the Linzizong volcanic successions over the southern Lhasa terrane (Pan et al., 2004; Lee, 2007).

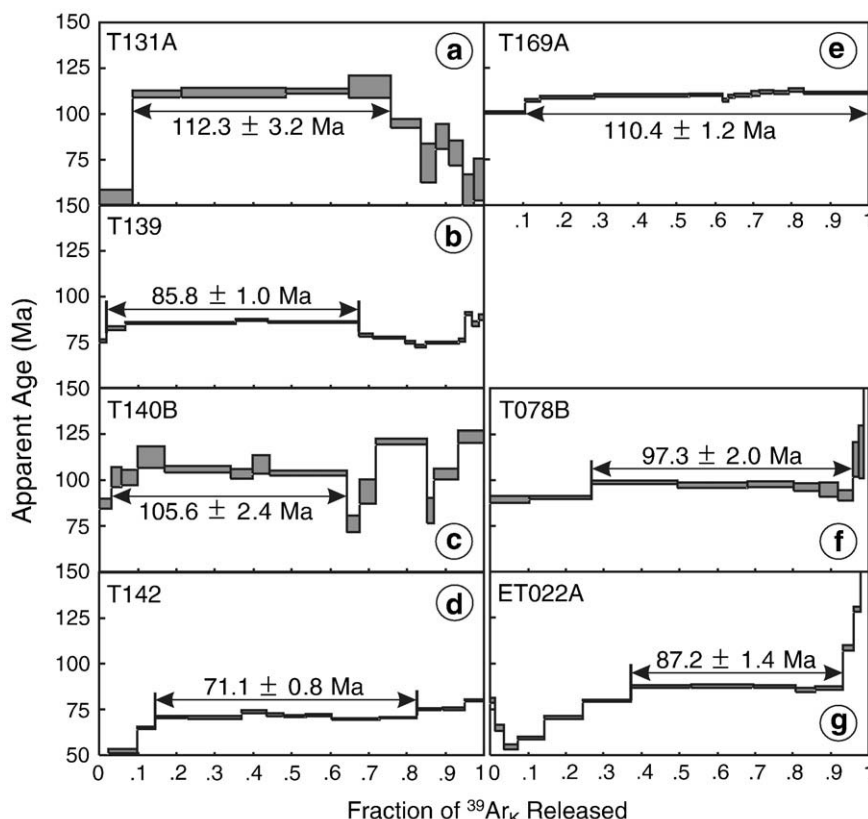


Fig. 3. Age spectra of 5 volcanic rocks (a to e) from the northern province and 2 others (f and g) from the Sangri Group. Plateau ages with 2σ analytical errors were calculated using the steps between arrows.

5.3. Magmatic flare-ups with heterogeneous compositions

The Linzizong volcanic successions consist dominantly of calc-alkaline rocks typical of arc lava geochemistry. This generality is, however, not persistent in volcanics produced during the flare-up period as their compositions vary from low-K tholeiitic through calc-alkaline to shoshonitic series (Fig. 5a). The compositional variations are furthermore associated with trace element and isotopic heterogeneities, i.e., each rock type has its own characteristic REE patterns (Fig. 5b) and Nd isotope ranges (Table 4), thus pointing to multiple source regions involved in the magma genesis at the particular moment (Lee, 2007). This requires a specific mechanism, other than the preexisting Neotethyan subduction that has long played a key role in generating the main suite of calc-alkaline rocks. By analogizing the better-studied example in the Mediterranean-Carpathian region (Wortel and Spakman, 2000; van de Zedde and Wortel, 2001; Coulon et al., 2002) and eastern Trans-Mexican Volcanic Belt (Orozco-Esquivel et al., 2007), and adopting the tectonic evolution scenarios described by Chung et al. (2005) in southern Tibet, we propose this mechanism to have been “shallow” breakoff of the steeply subducted Neotethyan oceanic slab (see below).

5.4. Rollback and breakoff of the Neotethyan subduction

Our observations of volcanic southward migration (Fig. 4; b and c) and intensification (Fig. 4c) in the Lhasa terrane lend important new constraints on the Himalayan-Tibetan tectonic evolution. The southward migration phenomenon strengthens the general notion for rollback and thus steepening of the Neotethyan subduction before the India-Asia collision starting presumably ca. 60–55 Ma (Fig. 6a; cf. Chung et al., 2005, for review). The subsequent intensification or,

more specifically, igneous flare-up event ca. 50 Ma, is related to breakoff of the steepened Neotethyan oceanic slab that occurred in the early stage of the India-Asia collision (Fig. 6b). Such a breakoff, i.e., detachment of the subducted oceanic lithosphere from its adhering continental lithosphere at “shallow” depths, would result in significant thermal perturbation to cause partial melting in various sources including the ascended asthenosphere, metasomatized domains in the continental lithospheric mantle, and even the overlying continental crust (van de Zedde and Wortel, 2001). Magmas generated under this condition, e.g., those in the Mediterranean-Carpathian region (Davies and von Blanckenburg, 1995; van de Zedde and Wortel, 2001; Coulon et al., 2002) are therefore typical of heterogeneous compositions that, as above-described, are also observed in southern Tibet during the magmatic flare-up period.

A shallow slab breakoff model can best explain the igneous flare-ups with compositional heterogeneity. This is manifested by the coexistence of 4 types of volcanic rocks in the Linzizong successions derived from different source regions (Fig. 6b). These are: (1) the main suite of calc-alkaline rocks with parental magmas originating from the mantle wedge and evolving by assimilation and fractional crystallization (AFC) processes; (2) the low-K tholeiitic suite that has the least-enriched LREE (Fig. 5b) and other incompatible trace elements, and highest Nd isotope ratios $\epsilon_{Nd}(T) \approx +3.5$; (Table 4), suggesting a juvenile mantle origin that can be attributed to decompressional melting of the upwelling asthenosphere; (3) the shoshonitic suite that has the most-enriched LREE (Fig. 5b) and other incompatible elements, but lower Nd isotope ratios $\epsilon_{Nd}(T) \approx -3$ to -5 ; (Table 4), interpreted as resulting from small-degree melting of the metasomatized lithospheric mantle source containing K-rich minerals such as amphibole or phlogopite (Tatsumi and Eggins, 1995); and (4) rhyolitic flows and ignimbrites marked by very evolved

Table 3

Summary of age data reported for volcanic rocks in the Lhasa terrane, southern Tibet.

	Locality	Sample	Rock type	Phase dated ^a	Ar-Ar (Myr ± 2σ)	Rb-Sr (Myr ± 2σ)	U-Pb (Myr ± 2σ)	Reference
Linzizong successions	Linzhou	XT 59	Andesite	Bt	59.3 ± 2			Maluski et al. (1982)
	Lhasa-Yangbajing	XGS-93	Ignimbrite	Bt, Fsp, WR		56.2 ± 1.4		Xu et al. (1985)
	Linzhou	T248	Andesite	Pl	49.2 ± 1			Coulon et al. (1986)
	NE Yangbajing	T286	Trachyte	Bt	50 ± 1			Coulon et al. (1986)
	SW Jarga	TE087/93	Dacite	Sa	44.8 ± 1.1			Miller et al. (2000)
	E Jarga	TE114/93	Dacite	Bt	54.1 ± 0.6			Miller et al. (2000)
	Linzhou	BD-114	Ignimbrite	WR	43.93 ± 0.52			Mo et al. (2003)
	Linzhou	BD-19	Rhyolite	Kfs	49.22 ± 0.72			Mo et al. (2003)
	Linzhou	D-15	Andesite	WR	60.63 ± 0.70			Mo et al. (2003)
	Linzhou	D-3	Andesite	Pl	64.47 ± 0.82			Mo et al. (2003)
	Linzhou	LZ-1	Ignimbrite	Kfs	48.73 ± 0.98			Mo et al. (2003)
	Linzhou	LZ9913	Andesite	Pl	61.45 ± 1.30			Mo et al. (2003)
	Linzhou	N-9	Andesite	Pl	56.51 ± 0.68			Mo et al. (2003)
	Linzhou	P-6-1	Rhyolite	WR	48.07 ± 0.42			Mo et al. (2003)
	Maqu	M-01	Andesite	WR	59.75 ± 1.08			Mo et al. (2003)
	Yangying	Y-5	Rhyolite	WR	52.91 ± 3.46			Mo et al. (2003)
	Linzhou	SH823034	Felsic tuff	Zr			47.1 ± 1.2	He et al. (2007)
	Linzhou	SH831031	Felsic tuff	Zr			53.9 ± 1.4	He et al. (2007)
	Linzhou	SH830034	Rhyolitic tuff	Zr			62.6 ± 2.4	He et al. (2007)
	Linzhou	SH530022	Rhyolite	Zr			68.7 ± 2.4	He et al. (2007)
	Linzhou	SH728032	Felsic dike	Zr			52.0 ± 1.0	He et al. (2007)
	Linzhou	SH522021	Felsic dike	Zr			51.7 ± 1.5	He et al. (2007)
	Linzhou	T233A	Breccia	Zr			62.5 ± 1.1	Lee et al. (2007)
	Linzhou	T235C	Ignimbrite	Zr			56.4 ± 1.2	Lee et al. (2007)
	Linzhou	ST053	Dacite	WR	47.1 ± 0.6			This study
	Linzhou	ST055A	Rhyolite	WR	49.3 ± 0.6			This study
	Linzhou	ST055C	Basaltic andesite	WR	43.8 ± 0.6			This study
	Linzhou	ST057A	Andesite	WR	46.5 ± 0.6			This study
	Linzhou	ST059A	Dacite	WR	48.8 ± 0.6			This study
	Linzhou	ST060C	Dacite	WR	48.7 ± 1.0			This study
	Linzhou	ST062	Dacite	WR	48.5 ± 0.8			This study
	Xigaze	T041F	Basaltic andesite	WR	49.3 ± 1.2			This study
	Nanmulin	T047	Basalt	WR	44.0 ± 0.8			This study
	Maijiang	T065A	Rhyolite	WR	48.6 ± 2.2			This study
	Maijiang	T068	Rhyolite	WR	47.8 ± 1.8			This study
	W Lhasa	T083C	Basalt	WR	43.2 ± 1.6			This study
	NE Majiang	T105A	Andesite	WR	53.0 ± 0.8			This study
	Jinda	T006B1	Basaltic andesite	WR	45.7 ± 1.8			This study
	N Sangsang	T038F	Dacite	WR	47.7 ± 2.2			This study
	N Sangsang	T038G	Dacite	WR	45.1 ± 1.6			This study
	Dajiaoc	T155	Dacite	WR	48.9 ± 0.8			This study
	NW Dajiaoc	T151	Dasalt	WR	53.9 ± 1.0			This study
	Comai	T136A	Rhyolite	WR	59.9 ± 0.8			This study
Northern province	Barda	T486	Andesite	Bt	112.3 ± 2.2			Coulon et al. (1986)
	Barda	T492	Dacite	Pl	90 ± 2			Coulon et al. (1986)
	Deqing	T468	Rhyolite	Pl	74.3 ± 4.3			Coulon et al. (1986)
	Jiangcuo	T398	Dacite	Pl	85 ± 2.2			Coulon et al. (1986)
	N Jiangcuo	T380	Andesite	Pl	90.5 ± 2.2			Coulon et al. (1986)
	Shenzha	T8284	Rhyolite	Pl	111.4 ± 2.6			Coulon et al. (1986)
	S Gaize	6-4-98-3d	Dacite	Bt	109 ± 1			Kapp et al. (2005)
	SE Gaize	6-6-98-2	Tuff	WR	110 ± 2			Kapp et al. (2005)
	N Nima	4MK175	Tuff	Zr			117 ± 2	Kapp et al. (2007b)
	S Nima	3MC13	Tuff	Zr			99 ± 2	Kapp et al. (2007b)
	Xiagangjiang	7-8-98-3	Tuff	Zr			106 ± 5	Volkmer et al. (2007)
	Xiagangjiang	8-18-03-2	Tuff	Zr			113 ± 10	Volkmer et al. (2007)
	N Comai	T131A	Rhyolite	WR	112 ± 3			This study
	Bangduo	T139	Rhyolite	WR	85.8 ± 1.0			This study
	Bangduo	T140B	Andesite	WR	106 ± 2			This study
Sangri Group	Coqin	T142	Dacite	WR	71.1 ± 0.8			This study
	Namuco	T169A	Rhyolite	WR	110 ± 1			This study
	NW Lhasa	T31	Andesite	Am	90 ± 2			Coulon et al. (1986)
	Lhasa-NE	T078B	Dacite	WR	97.3 ± 2.0			This study
	Qulong	ET022A	Rhyolite	WR	87.2 ± 1.4			This study

^a Bt: Biotite; Fsp: Feldspar; WR: Whole rock; Pl: Plagioclase; Sa: Sanidine; Kfs: K-feldspar; Zr: Zircon; Am: Amphibole.

compositions (e.g., $\text{SiO}_2 > 70$ wt.%) and the lowest Nd isotope ratios [e.g., sample T065A, with $\epsilon_{\text{Nd}}(\text{T}) \approx -13.7$, Table 4] that represent remelting products of the basement or continental crust of the Lhasa terrane.

We note that Mo et al. (2007, 2008) presented a different petrogenetic model by arguing that the Linzizong “syn-collisional” rocks were derived from mantle input in response to partial melting of

subducted Neotethyan oceanic crust with terrigenous sediments during the India–Asia collision. They proposed that the melts could have been “sustainably” generated by melting unusual “warm slabs” at the amphibolite facies condition. Such process seems to provide a possible mechanism for producing the voluminous andesitic or more silicic rocks that show mantle-dominated isotopic and geochemical signatures. However, it is uneasy if not unlikely to account for the

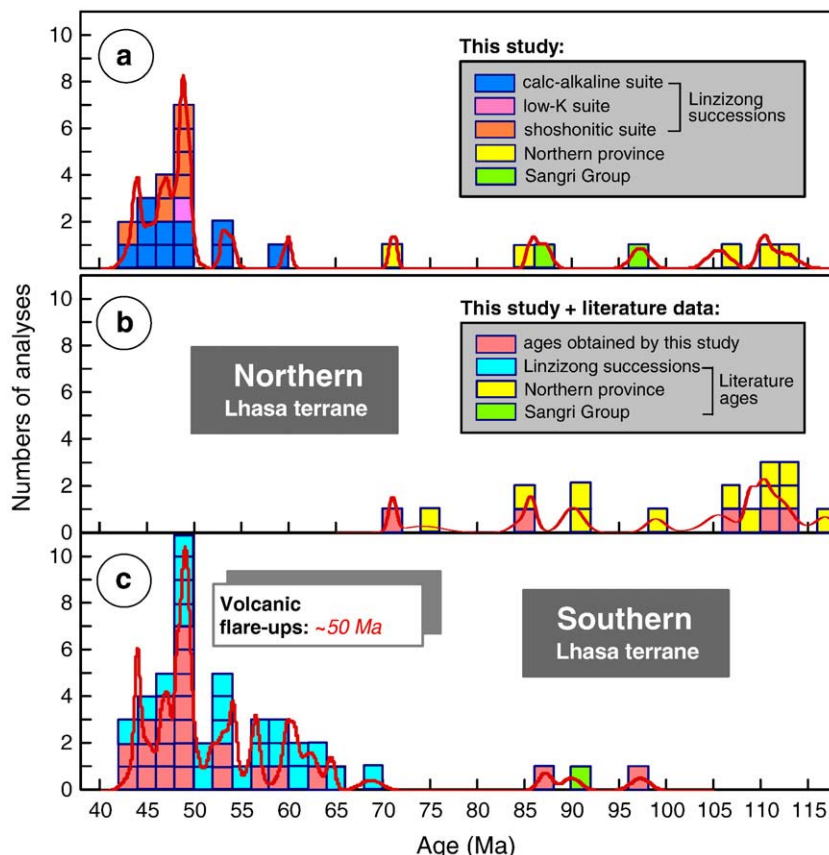


Fig. 4. Histograms of volcanic ages in the Lhasa terrane compiled from (a) this study, and all published age data from (b) northern Lhasa terrane and (c) southern Lhasa terrane. Literature data sources are given in Table 3.

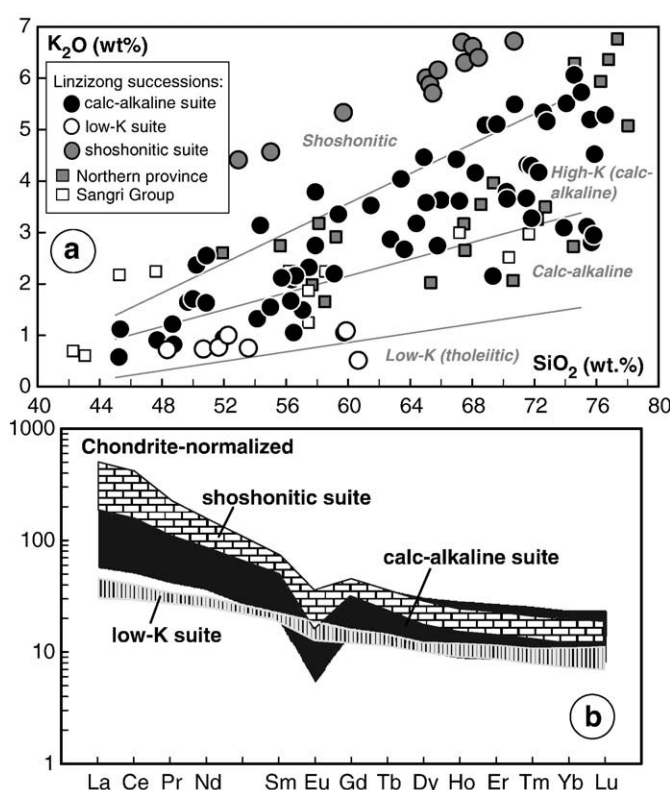


Fig. 5. (a) Plots of K_2O versus SiO_2 contents of the Linzizong and associated volcanic rocks. (b) Chondrite-normalized REE patterns of three principal magma suites formed during the flare-up period.

compositional heterogeneity observed by this study, and does not explain why a magmatic peak activity took place at ca. 50 Ma.

5.5. Supporting evidence and broader implications

While the proposed rollback and steepening of Neotethyan subduction is consistent with regional geologic data such as Cretaceous-Tertiary shortening and basin development history in central Tibet (Kapp et al., 2005), the idea of Eocene slab breakoff has also been advocated by previous workers using Himalayan metamorphic records (e.g., Kohn and Parkinson, 2002; Guillot et al., 2003). More specifically, in the western Himalaya, Leech et al. (2005) argued an early, steep continental attempted subduction to explain the occurrence and metamorphic ages (ca. 55–53 Ma) of coecite-bearing eclogites from the Tso Morari complex and suggested that oceanic slab breakoff broadly coincided with exhumation of the ultrahigh-pressure rocks in the region.

The breakoff, moreover, would have eliminated slab pull by the preexisting Neotethyan subduction and consequently prevented the Indian cratonic lithosphere, not only its crust but also its lithospheric mantle, from moving further downward so that terminated the attempted continental subduction (Chemenda et al., 2000). This is because the latter is more refractory and thus intrinsically more buoyant than the lithospheric mantle of the Lhasa terrane (Chung et al., 2005). Without any other place for the cold and hard Indian cratonic mantle to go, the continuous Indian northward pushing would have started causing distributed thickening of the Lhasa continental lithosphere, a process that eventually ceased the Linzizong/Gangdese magmatism ca. 45–43 Ma and led to the rise and growth of the southern Tibetan plateau (cf. Chung et al., 2005). Consequently, our Eocene slab breakoff model well explains why there

Table 4

Geochemical and Nd isotope data of representative samples from the Linzizong volcanic successions.

Sample	Calc-alkaline suite					Low-K suite		Shoshonitic suite		
	T047	T054A	T040A	T065A	T065B	T036D	T041F	ST055C	ST057A	ST060C
<i>Major elements (wt.%)</i>										
SiO ₂	50.87	56.49	64.39	73.90	75.87	48.34	52.25	52.92	59.69	68.39
TiO ₂	1.24	1.21	0.76	0.51	0.29	0.94	0.87	0.92	0.80	0.47
Al ₂ O ₃	22.41	17.64	16.60	10.87	13.82	18.65	19.20	17.49	17.64	15.16
Fe ₂ O ₃	7.53	8.92	4.60	3.95	2.16	10.52	10.57	7.96	5.82	2.51
MnO	0.11	0.19	0.10	0.07	0.03	0.16	0.14	0.17	0.07	0.08
MgO	2.75	2.74	1.56	2.26	0.22	6.18	3.84	4.10	2.11	0.81
CaO	6.33	7.09	3.45	1.80	1.15	9.28	7.23	6.34	4.21	1.35
Na ₂ O	4.25	3.19	3.91	1.00	2.77	3.31	3.06	2.66	2.83	2.82
K ₂ O	2.55	1.06	3.18	3.09	4.52	0.72	1.00	4.41	5.33	6.40
P ₂ O ₅	0.35	0.36	0.22	0.10	0.07	0.23	0.23	0.38	0.29	0.07
LO.I	0.96	0.71	1.31	1.91	0.94	0.51	1.63	2.97	0.87	0.84
Total	99.35	99.59	100.08	99.45	101.84	98.83	100.03	100.30	99.66	98.89
<i>Trace elements (ppm)</i>										
Sc	23.3	16.8	14.7	11.7	6.3	21.8	19.4	20.7	15.3	11.6
V	175	105	73.1	63.3	14.6	214	203	230	118	30.3
Cr	47.6	0.53	2.3	54.8	0.48	38.6	1.8	54.4	34.2	6.9
Co	16.7	13.6	7.8	9.7	1.9	29.8	23.0	25.2	9.2	3.2
Ni	18.8	1.9	2.4	22.5	1.5	24.0	7.3	28.9	15.1	5.1
Cu	5.8	6.3	8.6	18.3	6.8	50.0	21.3	12.0	13.0	2.5
Zn	83.2	110	59.1	86.2	45.4	68.5	63.5	164	63.9	63.8
Ga	24.5	19.5	18.7	15.8	15.8	18.9	19.8	21.1	21.0	19.3
Rb	120	33.6	110	131	183	19.7	21.3	160	252	426
Sr	445	557	453	108	131	746	703	1066	805	378
Y	26.1	27.7	24.8	26.2	29.6	14.7	15.4	29.0	28.5	39.7
Zr	89.5	108	127	72.8	78.6	12.1	31.9	139	250	254
Nb	10.1	5.2	10.0	12.9	13.6	2.2	1.9	7.8	13.7	24.6
Cs	18.3	4.8	5.3	7.9	7.0	1.1	1.1	5.7	9.4	12.0
Ba	459	290	545	483	470	229	275	657	849	219
La	26.3	18.1	30.3	35.3	36.0	7.96	8.46	46.8	58.6	89.2
Ce	55.3	40.7	61.9	70.6	65.3	19.0	19.1	93.5	117	198
Pr	6.64	5.35	7.09	7.85	8.39	2.66	2.62	10.3	12.4	17.8
Nd	27.6	23.8	27.5	29.1	30.7	12.6	12.1	41.3	46.6	62.1
Sm	5.79	5.49	5.37	5.46	5.55	3.05	2.86	8.22	8.60	10.7
Eu	1.54	1.66	1.31	1.06	0.81	1.01	1.13	2.19	2.23	1.15
Gd	5.65	5.47	5.01	5.13	5.28	2.98	2.80	7.22	7.26	8.92
Tb	0.86	0.88	0.74	0.77	0.79	0.48	0.45	1.04	1.00	1.25
Dy	4.69	4.95	4.00	4.22	4.40	2.67	2.58	5.35	5.05	6.46
Ho	0.96	1.03	0.82	0.87	0.95	0.56	0.54	1.01	0.96	1.26
Er	2.61	2.85	2.30	2.48	2.82	1.54	1.50	2.72	2.68	3.61
Tm	0.35	0.40	0.33	0.36	0.43	0.21	0.21	0.38	0.38	0.54
Yb	2.24	2.61	2.15	2.26	2.89	1.37	1.38	2.37	2.43	3.56
Lu	0.31	0.39	0.32	0.33	0.45	0.20	0.21	0.36	0.36	0.54
Hf	1.92	2.86	3.36	1.93	2.44	0.62	0.97	3.80	6.07	7.12
Ta	0.59	0.31	0.71	0.95	1.05	0.12	0.10	0.56	1.03	1.93
Pb	17.9	8.20	19.8	39.3	37.9	3.91	7.51	32.6	32.9	23.6
Th	0.57	1.21	0.88	15.4	21.1	1.48	8.33	10.1	27.3	54.5
U	1.03	0.70	2.51	2.01	2.17	0.23	0.13	2.12	4.83	8.24
ε_{Nd} (T)	0.3	-1.2	-1.0	-13.7	0.5	3.5	3.5	-2.8	-4.9	-4.6

Data from Lee (2007) PhD thesis, National Taiwan University. Major and trace elements were determined at National Taiwan University by X-ray fluorescence method using a Rigaku RIX-2000 spectrometer and by inductively coupled plasma-mass spectrometry using an Agilent 7500s quadrupole ICP-MS, respectively. The routine analytical precision and accuracy for most elements measured are estimated to be <5%. Nd isotope ratios were measured using Finnigan MAT 262 mass spectrometer at National Cheng-Kung University and Finnigan Neptune MC-ICP-MS at National Taiwan University. Detailed analytical procedures can be found in Wang et al. (2004) and Lee (2007).

was a decrease in the India-Asian convergence rate during Eocene time (Lee and Lawver, 1995).

Furthermore, slab breakoff could result in uplift in the topography. Our model therefore suggests not only a significant Eocene tectono-magmatic activity in southern Tibet but also a concomitant uplift in the region. This argument is supported by several sedimentary records. Based on an oxygen-isotope-based study of the paleo-altimetry of sedimentary basins from southern Tibet, Rowley and Currie (2006) concluded that the surface elevations of 4 km or more were established before 40 Ma. A similar conclusion has been proposed by Wang et al. (2008) that reviewed numerous geologic and geophysical data over the Tibetan plateau. An Eocene uplift interpretation is also consistent with deposition of the youngest marine strata during ~52–45 Ma in the Tethyan Himalaya (Dewey

et al., 1988; Gaetani and Garzanti, 1991; Rowley, 1996). Voluminous sediments eroded from the uplifted orogen may be best illustrated by the thick piles of deposition in the Bengal basin, in which a noticeable change in basin configuration took place in early Eocene time, associated with a drastic increase in the sediment flux and development of prograding clastic depositional sequences (Lindsay et al., 1991; Alam et al., 2003).

Lastly, this study reinforce the argument by Chung et al. (2005) who suggested an Eocene slab breakoff followed by removal of collision-thickened Lhasa lithospheric root ca. 25 Ma. This double detachment scenario is compatible with the suggestion based on regional seismic tomography (Van der Voo et al., 1999) that, by contrast, was taken as supporting evidence for widespread occurrence of an intraoceanic arc system that collided with northern India ca. 55 Ma followed by a much

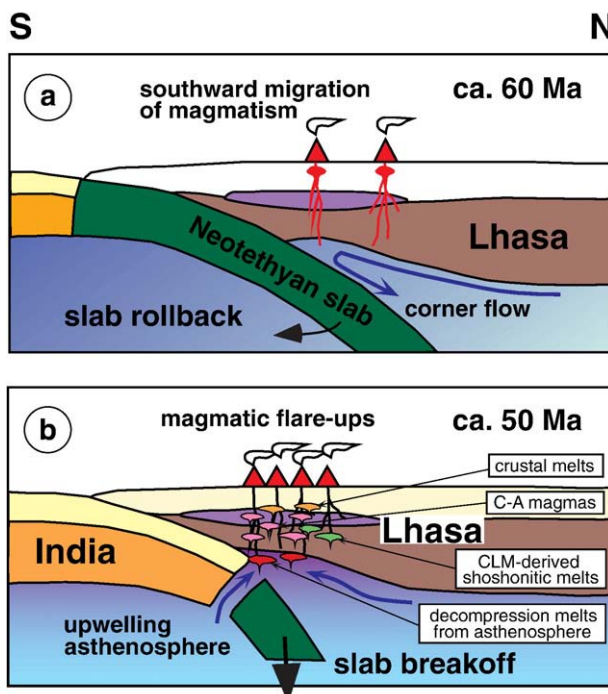


Fig. 6. Schematic models for (a) rollback and (b) breakoff of the Neotethyan slab in southern Tibet. The latter mechanism would result in the magmatic flare-ups originating from various sources. C-A = calc-alkaline; CLM = continental lithospheric mantle. See text for detailed discussion.

younger continent-continent collision between India and Asia in the Oligocene (cf. Aitchison et al., 2007). We agree with these authors on their point of critical reassessment of existing hypotheses regarding the India–Asia collision, but address that the “double collision” model did not and can hardly account for the southward migration and intensification of the volcanism in southern Tibet.

6. Concluding remarks

In this study, we report new $^{40}\text{Ar}/^{39}\text{Ar}$ age results that allow a better understanding of the temporal-spatial distribution of the Linzizong volcanism. The age data delineate two discrete episodes of volcanic activity in southern Tibet. These are (1) a widespread Cretaceous episode, and (2) an intense, but geographically confined, Paleogene episode that occurred only in the southern part of the Lhasa terrane. The second episode is here re-defined as the “real” Linzizong volcanic successions. The age data furthermore indicate a southward migration and intensification of the volcanism, which culminated at ca. 50 Ma and resulted in a magmatic “flare-up” period in the southern Lhasa terrane.

The Linzizong volcanic successions consist dominantly of calc-alkaline rocks that range from basalt to rhyolite compositions and are characterized by typical arc-lava geochemical features. Those formed during the flare-up period, however, show significant geochemical variations from low-K tholeiitic through calc-alkaline to shoshonitic compositions, implying involvement of heterogeneous mantle and/or crustal source regions in the petrogenesis that would require a different magma generation mechanism rather than the normal Neotethyan subduction.

We interpret the southward migration and subsequent flare-ups of the volcanism as the consequences of rollback and breakoff, respectively, of the Neotethyan subducted slab that took place before and in the early stage of the India–Asia collision. The timing of Neotethyan slab breakoff may be best constrained by the magmatic flare-ups event at ca. 50 Ma. The slab breakoff would have resulted in

significant asthenospheric upwelling and caused partial melting in not only the ascended asthenosphere but also the overlying metasomatized lithospheric mantle and crust, which accounted for the geochemical heterogeneities of the magmas formed.

Acknowledgments

We thank D.-R. Wen, M.-F. Chu and D.-C. Zhu for help in the field work and sharing data/ideas. Careful and constructive reviews by two anonymous journal reviewers helped improve the presentation of the paper. This study benefited from financial supports by the National Science Council, Taiwan, ROC.

References

- Aitchison, J.C., Ali, J.R., Davis, A.M., 2007. When and where did India and Asia collide? *Journal of Geophysical Research* 112, B05423. doi:10.1029/2006JB004706.
- Alam, M., Alam, M.M., Curraj, J.R., Chowdhury, M.L.R., Gani, M.R., 2003. An overview of the sedimentary geology of the Bengal Basin in relation to the regional tectonic framework and basin-fill history. *Sedimentary Geology* 155, 179–208.
- Chemenda, A.I., Burg, J.-P., Mattauer, M., 2000. Evolutionary model of the Himalaya-Tibet system: geopoem based on new modeling, geological and geophysical data. *Earth and Planetary Science Letters* 174, 397–409.
- Chung, S.-L., Chu, M.-F., Zhang, Y., Xie, Y., Lo, C.-H., Lee, T.-Y., Lan, C.-Y., Li, X., Zhang, Q., Wang, Y., 2005. Tibetan tectonic evolution inferred from spatial and temporal variations in post-collisional magmatism. *Earth-Science Reviews* 68, 173–196.
- Coulon, C., Maluski, H., Bollinger, C., Wang, S., 1986. Mesozoic and Cenozoic volcanic rocks from central and southern Tibet: $^{39}\text{Ar}/^{40}\text{Ar}$ dating, petrological characteristics and geodynamical significance. *Earth and Planetary Science Letters* 79, 281–302.
- Coulon, C., Megartsi, M., Fourcade, S., Maury, R.C., Bellon, H., Louhi-Hacini, A., Cottet, J., Coutelle, A., Hermitte, D., 2002. Post-collisional transition from calc-alkaline to alkaline volcanism during the Neogene in Oranie (Algeria): magmatic expression of a slab breakoff. *Lithos* 62, 87–110.
- Davies, J.H., von Blanckenburg, F., 1995. Slab breakoff: a model of lithosphere detachment and its test in the magmatism and deformation of collisional orogens. *Earth and Planetary Science Letters* 129, 85–102.
- DeCelles, P.G., Robinson, D.M., Zandt, G., 2002. Implications of shortening in the Himalayan fold-thrust belt for uplift of the Tibetan plateau. *Tectonics* 21, 1062. doi:10.1029/2001TC001322.
- Dewey, J.F., Shackleton, R.M., Chang, C., Sun, Y., 1988. The tectonic evolution of the Tibetan plateau. *Royal Society of London Philosophical Transactions* 327, 379–413.
- Dong, G., Mo, X., Zhao, Z., Wang, L., Zhou, S., 2005. A new understanding of the stratigraphic successions of the Linzizong volcanic rocks in the Linzhou Basin, Tibet. *Geological Bulletin of China* 24, 549–557.
- Fleck, R.J., Sutter, J.F., Elliot, D.H., 1977. Interpretation of discordant $^{40}\text{Ar}/^{39}\text{Ar}$ age spectra of Mesozoic tholeiites from Antarctica. *Geochimica et Cosmochimica Acta* 41, 15–32.
- Gaetani, M., Garzanti, E., 1991. Multicyclic history of the northern India continental margin (Northwestern Himalaya). *American Association of Petroleum Geologists Bulletin* 75, 1427–1446.
- Guillet, S., Garzanti, E., Baratoux, D., Marquer, D., Mahéo, G., de Sigoyer, J., 2003. Reconstructing the total shortening history of the NW Himalaya. *Geochemistry, Geophysics, Geosystems* 4. doi:10.1029/2002GC000484.
- He, S., Kapp, P., DeCelles, P.G., Gehrels, G.E., Heizler, M., 2007. Cretaceous–Tertiary geology of the Gangdese Arc in the Linzhou area, southern Tibet. *Tectonophysics* 433, 15–37.
- Kapp, P., Yin, A., Harrison, T.M., Ding, L., 2005. Cretaceous–Tertiary shortening, basin development, and volcanism in central Tibet. *Geological Society of America Bulletin* 117, 865–878.
- Kapp, P., DeCelles, P.G., Leier, A.L., Fabijanic, J.M., He, S., Pullen, A., Gehrels, G.E., 2007a. The Gangdese retroarc thrust belt revealed. *GSA Today* 17, 4–9.
- Kapp, P., DeCelles, P.G., Gehrels, G.E., Heizler, M., Ding, L., 2007b. Geological records of the Lhasa-Qiangtang and Indo-Asian collisions in the Nima area of central Tibet. *GSA Bulletin* 119, 917–932.
- Kohn, M.J., Parkinson, C.D., 2002. Petrologic case for Eocene slab breakoff during the Indo-Asian collision. *Geology* 30, 591–594.
- Lee, H.-Y., 2007. The Linzizong Volcanic Successions, Southern Tibet: Ages, Geochemical Characteristics and Petrogenesis. Ph.D. Thesis, National Taiwan University.
- Lee, T.-Y., Lawyer, L.A., 1995. Cenozoic plate reconstruction of Southeast Asia. *Tectonophysics* 251, 85–138.
- Lee, H.-Y., Chung, S.-L., Wang, J.-R., Wen, D.-J., Lo, C.-H., Yang, T.F., Zhang, Y., Xie, Y., Lee, T.-Y., Wu, G., Ji, J., 2003. Miocene Jiali faulting and its implications for Tibetan tectonic evolution. *Earth and Planetary Science Letters* 205, 185–194.
- Lee, H.-Y., Chung, S.-L., Wang, Y., Zhu, D., Yang, J., Song, B., Liu, D., Wu, F., 2007. Age, petrogenesis and geological significance of the Linzizong volcanic successions in the Linzhou Basin, southern Tibet: evidence from zircon U-Pb dates and Hf isotopes. *Acta Petrologica Sinica* 23, 493–500.
- Leech, M.L., Singh, S., Jain, A.K., Klempert, S.L., Manickavasagam, R.M., 2005. The onset of India–Asia continental collision: early, steep subduction required by the timing of UHP metamorphism in the western Himalaya. *Earth and Planetary Science Letters* 234, 83–97.

- Leier, A.L., DeCelles, P.G., Kapp, P., Ding, L., 2007. The Takena Formation of the Lhasa terrane, southern Tibet: the record of a Late Cretaceous retroarc foreland basin. *Geological Society of America Bulletin* 119, 31–48.
- Lindsay, J.F., Holliday, D.W., Hulbert, A.G., 1991. Sequence stratigraphy and evolution of Ganges–Brahmaputra Delta complex. *American Association of Petroleum Geologists Bulletin* 75, 1233–1254.
- Lo, C.-H., Chung, S.-L., Lee, T.-Y., Wu, G., 2002. Age of the Emeishan flood magmatism and relations to Permian–Triassic boundary events. *Earth and Planetary Science Letters* 198, 449–458.
- Mahéo, G., Guillot, S., Blichert-Toft, J., Rolland, Y., Pêcher, A., 2002. A slab breakoff model for the Neogene thermal evolution of South Karakoram and South Tibet. *Earth and Planetary Science Letters* 195, 45–58.
- Maluski, H., Proust, F., Xiao, X.C., 1982. $^{39}\text{Ar}/^{40}\text{Ar}$ dating of the trans-Himalayan calc-alkaline magmatism of southern Tibet. *Nature* 298, 152–154.
- Miller, C., Schuster, R., Klötzli, U., Frank, W., Purtscheller, F., 1999. Post-collisional potassic and ultrapotassic magmatism in SW Tibet: geochemical and Sr–Nd–Pb–O isotopic constraints for mantle source characteristics and petrogenesis. *Journal of Petrology* 40, 1399–1424.
- Miller, C., Schuster, R., Klötzli, U., Frank, W., Grasemann, B., 2000. Late Cretaceous–Tertiary magmatic and tectonic events in the Transhimalaya batholith (Kailas area, SW Tibet). *Schweizerische Mineralogische und Petrographische Mitteilungen* 80, 1–20.
- Mo, X., Zhao, Z., Deng, J., Dong, G., Zhou, S., 2003. Response of volcanism to the India–Asia collision. *Earth Science Frontiers* 10, 135–147.
- Mo, X., Hou, Z., Niu, Y., Dong, G., Qu, X., Zhao, Z., Yang, Z., 2007. Mantle contributions to crustal thickening during continental collision: evidence from Cenozoic igneous rocks in southern Tibet. *Lithos* 96, 225–242.
- Mo, X., Niu, Y., Dong, G., Zhao, Z., Hou, Z., Zhou, S., Ke, S., 2008. Contribution of syncollisional felsic magmatism to continental crust growth: a case study of the Paleogene Linzizong Volcanic Succession in southern Tibet. *Chemical Geology* 250, 49–67. doi:[10.1016/j.chemgeo.2008.02.003](https://doi.org/10.1016/j.chemgeo.2008.02.003).
- Murphy, M.A., Yin, A., Harrison, T.M., Dürr, S.B., Chen, Z., Ryerson, F.J., Kidd, W.S.F., Wang, X., Zhou, X., 1997. Did the Indo–Asian collision alone create the Tibetan plateau? *Geology* 25, 719–722.
- Orozco-Esquivel, T., Petrone, C.M., Ferrari, L., Tagami, T., Manetti, P., 2007. Geochemical and isotopic variability in lavas from the eastern Trans-Mexican Volcanic Belt: slab detachment in a subduction zone with varying dip. *Lithos* 93, 149–174.
- Pan, G., Ding, J., Yao, D., Wang, L., compilers, 2004. The Guide Book of 1:1,500,000 Geologic Map of the Qinghai-Xizang (Tibet) Plateau and Adjacent Areas. Chengdu Cartographic Publishing House. 48 pp.
- Renne, P.R., Swisher, C.C., Deino, A.L., Karner, D.B., Owens, T.L., DePaolo, D.J., 1998. Intercalibration of standards, absolute ages and uncertainties in $^{40}\text{Ar}/^{39}\text{Ar}$ dating. *Chemical Geology* 145, 117–152.
- Rowley, D.B., 1996. Age of initiation of collision between India and Asia: a review of stratigraphic data. *Earth and Planetary Science Letters* 145, 1–13.
- Rowley, D.B., Currie, B.S., 2006. Palaeo-altimetry of the Late Eocene to Miocene Lunpola Basin, central Tibet. *Nature* 439, 677–681. doi:[10.1038/nature04506](https://doi.org/10.1038/nature04506).
- Steiger, R.H., Jäger, E., 1977. Subcommission on geochronology: convention on the use of decay constants in geo- and cosmochronology. *Earth and Planetary Science Letters* 36, 359–362.
- Tatsumi, Y., Eggins, S., 1995. Subduction Zone Magmatism. Blackwell Science Publication. 211 pp.
- van de Zedde, D.M.A., Wortel, M.J.R., 2001. Shallow slab detachment as a transient source of heat at midlithospheric depths. *Tectonics* 20, 868–882.
- Van der Voo, R., Spakman, W., Bijwaard, H., 1999. Tethyan subduction slabs under India. *Earth and Planetary Science Letters* 171, 7–20.
- Volkmer, J.E., Kapp, P., Guynn, J.H., Lai, Q., 2007. Cretaceous–Tertiary structural evolution of the north central Lhasa terrane, Tibet. *Tectonics* 26. doi:[10.1029/2005TC001832](https://doi.org/10.1029/2005TC001832).
- Wang, K.-L., Chung, S.-L., O’Reilly, S.Y., Sun, S.-s., Shinjo, R., Chen, C.-H., 2004. Geochemical constraints for the genesis of post-collisional magmatism and the geodynamic evolution of the northern Taiwan region. *Journal of Petrology* 45, 975–1011.
- Wang, C., Zhao, X., Liu, Z., Lippert, P.C., Graham, S.A., Coe, R.S., Yi, H., Zhu, L., Liu, S., Li, Y., 2008. Constraints on the early uplift history of the Tibetan plateau. *Proceedings of the National Academy of Sciences* 105, 4987–4992.
- Wen, D.-R., Liu, D., Chung, S.-L., Chu, M.-F., Ji, J., Zhang, Q., Song, B., Lee, T.-Y., Yeh, M.-W., Lo, C.-H., 2008. Zircon SHRIMP U–Pb ages of the Gangdese Batholith and implications for Neotethyan subduction in southern Tibet. *Chemical Geology* 252, 191–201.
- Wortel, M.J.R., Spakman, W., 2000. Subduction and slab detachment in the Mediterranean–Carpathian region. *Science* 290, 1910–1917.
- Xu, R.-H., Schärer, U., Allègre, C.J., 1985. Magmatism and metamorphism in the Lhasa block (Tibet): a geochronological study. *Journal of Geology* 93, 41–57.
- Yin, A., Harrison, T.M., 2000. Geologic evolution of the Himalayan–Tibetan orogen. *Annual Review of Earth and Planetary Sciences* 28, 211–280.
- Zhu, D.-C., Zhao, Z.-D., Pan, G.-T., Lee, H.-Y., Kang, Z.-Q., Liao, Z.-L., Wang, L.-Q., Li, G.-M., Dong, G.-C., Liu, B., 2009. Early Cretaceous subduction-related adakite-like rocks of the Gangdese Belt, southern Tibet: Products of slab melting and subsequent melt–peridotite interaction? *Journal of Asian Earth Sciences* 34, 298–309.